Multiple Subbands Ranging Signals Design and Investigation on Frequency Dependence of the Subband Channel Impulse Responses within an Ultra-wideband Channel

Thesis

submitted in partial fulfillment of the
requirements for the degree of

Master of Science

in

Electrical Engineering

by

Xiaoyao Luo
born in Qianjiang, China

This work was performed in:

Circuits and Systems Group
Department of Microelectronics & Computer Engineering
Faculty of Electrical Engineering, Mathematics and Computer Science
Delft University of Technology

Delft University of Technology

Delft University of Technology
Department of
Microelectronics & Computer Engineering

The undersigned hereby certify that they have read and recommend to the Faculty of Electrical Engineering, Mathematics and Computer Science for acceptance a thesis entitled **"Multiple Subbands Ranging Signals Design and Investigation on Frequency Dependence of the Subband Channel Impulse Responses within an Ultra-wideband Channel"** by **Xiaoyao Luo** in partial fulfillment of the requirements for the degree of **Master of Science**.

Dated: 16.05.2022

Chairman: ____________________
dr.ir. G.J.M. Janssen

Advisor: ____________________
dr.ir. G.J.M. Janssen

Committee Members: ____________________
dr.ir. J. Romme

____
dr. O.A. Krasnov

Abstract

This thesis covers two topics. The first one is signal design for accurate Time-of-Arrival estimation using a number of frequency separated signals. Rather than use a full UWB band, we will use sparse subband signals spanning the full band to construct a new virtual UWB signal. To evaluate the performance of the constructed signal, Cramer-Rao lower bound and auto-correlation are used. And given a given fixed bandwidth the number of subbands within a 1 GHz UWB channel, and optimal subbands' allocation will be found based on the evaluation results.

Our results show that when three 50 MHz subbands are used to construct a virtual 1GHz UWB signal, a lower CRLB and better auto-correlation performance can be reached when subbands are close to the edges of the virtual band. However, the auto-correlation still has multiple peaks, which poses a serious challenge for accurate time estimation.

The second topic is to investigate the frequency dependence of the channel impulse response of subbands with different frequency separations. We propose a covariance calculation method to determine the frequency dependence which changes with frequency separation.

To validate the method, different artificial UWB channels with distinct paths are given. The results show that covariances between the subband CIRs stay at a high level when measured at the direct path and the majority of interference caused by other paths can be eliminated by a wider bandwidth subband. Given UWB channels measured from 5 to 10 GHz with a link-budget of 120dB, the frequency dependence of the direct path and reflections are determined, different bandwidths and frequency separations are used, and the results show that the channel impulse response of the subbands will become different when measured at different center frequencies, where the difference increases with an increased frequency separation of the subbands. The correlation of the direct path is maintained over larger frequency distances than that of reflected paths.

Index Terms — Ultra-wideband, Subbands, Cramer-Rao Lower Bound, Frequency dependence, Multipath

Acknowledgments

In the past almost 1,000 days, from normal campus life to the epidemic life of staying completely at home, offline classes, online classes, written tests, and oral exams. It's a little unreal to look back on. These days were filled with joy, frustration, and various other emotions, but in the end, they were all a valuable and everlasting experience.

I would like to express my gratitude to my respectful supervisor, dr.ir. Gerard Janssen. Without his kindness and patience, I could not finish this thesis report. Throughout the process, I encountered many difficulties. Thanks to discussions with my professor time and again, I could solve them. Especially sometimes I would send emails to him during non-working hours, even then, my professor would answer my questions as soon as possible. And he also cared about my physical and mental health during the whole epidemic, it was my honor to work with such a professor. I also want to thank dr.ir. J. Romme and Imec Netherlands for providing the measurements I use in this report, and thank dr.ir. J. Romme and dr. O.A. Krasnov for being my thesis committee members.

I would also like to express my gratitude to my friends in other countries. Although we are in the Netherlands, in the United Kingdom, in the United States, and in China, the geographical distance does not hinder our communication. Having you all with me when I felt physically and mentally exhausted always helped me recover and keep an optimistic attitude throughout the pandemic.

And also I want to thanks some people I met in Netherlands, my Indian neighbors, intern colleagues, classmates, and some strangers who show me kindness, these people made my life here colorful. And my friends I knew here, thanks for the great days of playing badminton, finding delicious restaurants, travelling or just chatting with your guys.

Last but not least, my parents, thanks for you kindness and both physical and mental support in last 25 years, I will always be grateful for you giving me the freedom to choose the life I want.

Xiaoyao Luo
Delft, The Netherlands
16.05.2022

Contents

Acronyms

Time of Arrival	TOA
Line of Sight	LoS
Ultra-wideband	UWB
Probability Density Function	PDF
Power Spectrum Density	PSD
Cramer-Rao Lower Bound	CRLB
Root Mean Square	RMS
Channel Impulse Response	CIR

Table 0.1: Acronyms

Introduction

1

1.1 Background

Over the past decades, wireless technologies have become a part of human life and they are continuously evolving. Different wireless technologies show up everywhere in our daily life, such as Mobile Phones, Global Position System, Remote Controls, Bluetooth Audio and Wi-Fi etc. A basic wireless communication system consists of three parts, transmitter, channel and receive.

In recent years, positioning and ranging technology based on wireless communication has become a popular field of research that has attracted the attention of many scientists. The most successful use case is the Global Positioning System (GPS), with more than 30 navigation satellites circling the Earth as transmitters. The GPS receivers can receive the signals and measure the distances between the transmitters and the receiver, and based on this determine the location of the receiver. A lot of algorithms are proposed to process the received signals and precisely determine the location. Time of Arrival (ToA) estimation is quite popular among these studies, which measures the distance of the Line of Sight (LoA) path between transmitter and receiver based on the accurate time delay estimation. But in practice, besides the LoS path, there are other signals received through the reflected paths which interfere the direct path delay estimation, as shown in figure 1.1.

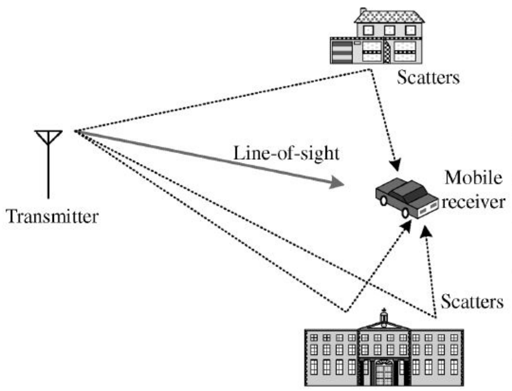

Figure 1.1: LOS in practice

In real environments, like built-up areas (urban canyons) and indoor, there is quite a large number of paths, and these situations pose a serious challenge on positioning system like GPS. Paths can not be distinguished since the delay time differences between different paths are quite small. And in order to deal with these situations, higher accuracy TOA estimation is of vital importance to improve the accuracy of positioning systems. High accuracy TOA estimation requires high time resolution, which is inversely proportional to the bandwidth of the used signal, and a quite wide bandwidth should be used to achieve decimeter accuracy ranging and positioning. Therefore, researchers gradually focus on improving the delay estimation accuracy, such as designing new spread spectrum signals, using large bandwidth like wider ultra-wideband signals and more.

1.2 Motivation

In positioning systems, time delay estimation is the most straightforward method to obtain range information which can be used for navigation and position. The Cramer-Rao Bound is a valid evaluation standard on the sync performance of the positioning signal, which is directly related to practical signal lock schemes [1]. Thus, the time delay estimation optimization problem becomes a problem to find the lower Cramer-Rao Bound. This paper concludes that current ranging signals used in GALILEO and GPS-II still can not have the same performance as the theoretical optimum pulse considering practical band limitations of the satellite transponder. Similarly, maximization of the Gabor bandwidth is shown to improve the delay estimation accuracy effectively with a fixed narrow signal bandwidth [2]. Bandwidth limitation is a vital challenge for ranging accuracy improvement, which directly influences the ability to distinguish the direct path from close reflections. It is shown that when two different signals broadcast on different carrier frequencies are processed as a single signal with only one center frequency, it outperforms than only single signal is processed on multipath rejection, resulting in a higher accuracy time delay estimation [3]. Alternatively, large signal bandwidth is potentially available in a terrestrial positioning system such as an UWB signal.

UWB, which occupies 500 MHz or more, gains more and more attention in recent years. At 2009, an overview of UWB propagation channels have been given by Molish, pointing out that the UWB channel can resolve more close-in paths than conventional (narrow-band and wide-band) propagation channels [4]. Different multipath components can be easily distinguished in the time domain because of the large bandwidth.

However, it will cost too much spectrum usage and increased sample rate for wide bandwidth signals requires substantial processing power. The above researches give us an idea on how to solve this problem. If the receiver receives a sparse subband signal on different frequencies spaning an UWB channel, where only part of the UWB channel would be used, does the combined signals have similar performance as the UWB signals, and how about the impact caused by the different subband allocation.

Then we look at some studies that focus on UWB channel, researchers have analysed subband-level frequency-dependent propagation inside an UWB channel [5], concluding that both delay and angular spreads shows significant differences when measured at different frequencies within an UWB channel. Study [6] shows that there is spectral distortion caused by the power and pathloss variation with frequency. But when the UWB channels are used in practice, given an UWB channel measured from 5 to 10 GHz, the increase of the bandwidth from 500MHz to 1.5GHZ of a subband with carrier frequency 8GHz does not improve the mean localization accuracy [7]. Therefore, here comes the question that what is the difference between the subbands with different carrier frequencies inside an UWB channel, does the CIR of subbands shows frequency dependence on the different carrier frequencies. Taking multipath components into account, we are curious about the frequency dependence of different paths in the CIRs of subbands.

1.3 Research Statement

This thesis covers two topics, the first one is signal design for accurate Time-of-Arrival estimation using a number of frequency separated signals. Using sparse subband signals, the main goal for this topic is to investigate the error caused by the constructed signal from subbbands compared to a full UWB signal, find the trade-off that can be made between ToA estimation accuracy and subband allocation.

And the second topic is to investigate the frequency dependence of the channel impulse response of the subband with different frequency separations. A method is proposed to determine the frequency dependence of the channel impulse response of subbands. How the method performs when different UWB channels are given? What is the frequency dependence of different paths in time domain?

1.4 Outline

This thesis report is structured as follows.

- Chapter 2 presents a description of a multiple subbands UWB signal model and frequency dependence model.
- Chapter 3 presents the mathematical expression of the multiple subbands UWB signal, gives the detailed mathematical derivation of the Cramer-Rao Lower Bound and auto-correlation.
- Chapter 4 presents the results of the Cramer-Rao Lower Bound and auto-correlation when using different vitrual UWB signals. The performance of the constructed signals is determined for different subband allocation schemes.
- Chapter 5 introduces the frequency dependence of the channel impulse responses of subbands within an UWB channel and mathematical expressions are given, proposed to determine the frequency dependence.
- Chapter 6 presents the results of the frequency dependence model, analyses the results for different UWB channels, and discuss the frequency dependence of different paths within an UWB channel.
- Chapter 7 presents the conclusions of this thesis.

System Description

2

In this chapter, we will give the basic idea for both two topics, and system models we use for the virtual UWB channel and signal are presented.

2.1 Introduction

Given a general model, if there is a signal or channel with a large bandwidth in the frequency domain, it can be seen as the combination of many subbands signals and channels as shown in the figure 2.1.

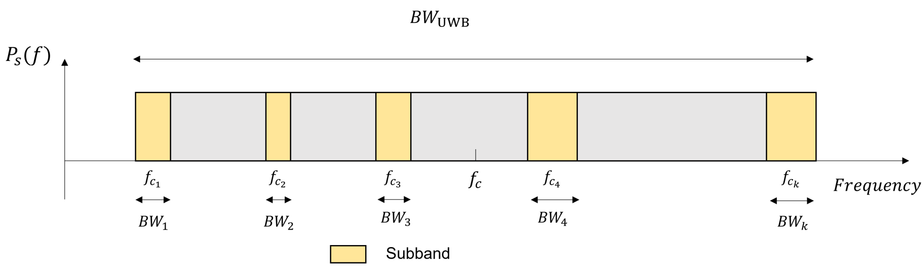

Figure 2.1: General model for an UWB spectrum

In this figure, subbands BW_1 through BW_K, the parts in yellow, are used for transmission. The full spectrum spans a virtual bandwidth $BW_{virtual} = f_{c_k} - f_{c_1} + \frac{BW_1}{2} + \frac{BW_K}{2}$, and the subbands might have different bandwidths, different center frequencies, and also different channel characteristics. In the following sections, we will give more detailed models for our topics.

2.2 Model of a multiple subband ultra wideband signal

In this model, we try to take advantage of the large bandwidth BW_{UWB} when only the yellow parts are what we really can obtain. Then the question becomes that how the assigned allocation of subbands can achieve a similar performance as what we use the full virtual bandwidth, especially when the signal is applied for ToA estimation.

Assuming the virtual bandwidth of the signal is BW_{UWB} and its spectrum is centered at f_c, a series of subbands centered at $f = f_{c_k}$ with bandwidth BW_k are what we really use. To simplify the model in advance, rectangular shapes are used to represent the Power Spectrum Density in the following figure.

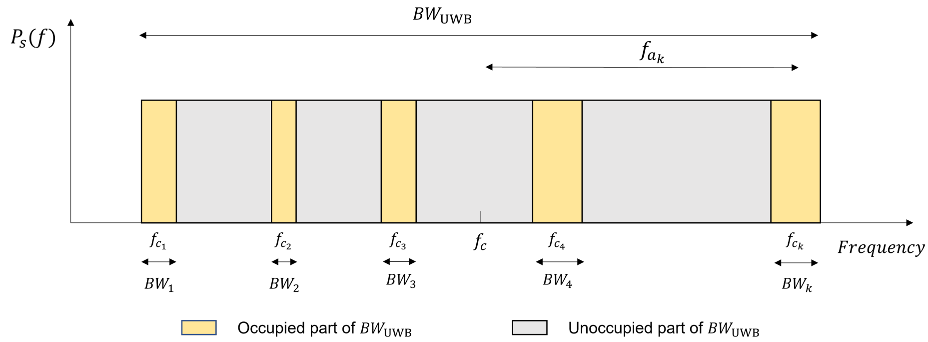

Figure 2.2: Diagram of the PSD of a sparse multi-band signal with a center frequency f_c .Only the parts in yellow, subbands BW_1 to BW_k, are occupied.

In figure 2.2, sparse subbands are spread over a much wider bandwidth BW_{UWB}. The subbands only occupy a fraction of the whole band, thus we can have a virtual signal spanning a virtual bandwidth with these known subbands.

Then we use the subbands signals to represent the virtual signal. Considering there are K baseband subband signals which has bandwidth BW_k, where $k = 1, 2, ..., K$. Therefore, K subband signals with their spectrum centered at f_{a_k} are defined by the equation (2.1) and shown in figure 2.3.

$$x_k(t) = x_k^{bb}(t)e^{j2\pi f_{a_k} t} \tag{2.1}$$

where $x_k^{bb}(t)$ is the kth subband signal with bandwidth BW_k in baseband, and k represents the kth subband, and $x_k(t)$ is the subband signal centered at f_{a_k}.

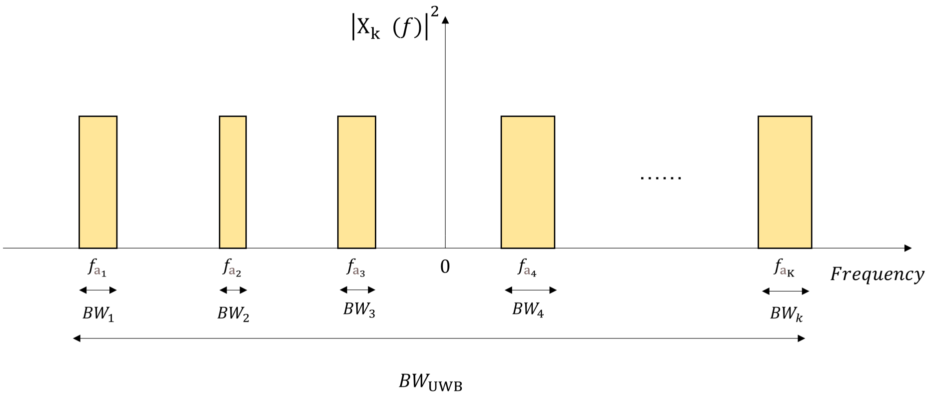

Figure 2.3: Spectrum of a series of signals

Here we assume that the PSDs of the subband signals have constant values to simplify the model, however this is not the case in practice. In this case, virtual signal $s(t)$ can be seen as a bandpass signal that filter out the unoccupied parts inside the full channel, and can be written as the sum of subband signals.

$$s(t) = \sum_{k=1}^{K} x_k^{bb}(t)e^{j2\pi f_{a_k} t} \tag{2.2}$$

2.3 Frequency dependence model

In this model, instead of constructing the signal from known subbands, we focus on the frequency dependency of the impulse response of subbands centered at different frequencies inside the full band channel.

Given an UWB channel starts at f_l, ends at f_h with a bandwidth BW_{UWB} in the frequency domain, since the channel impulse responses can be obtained by the inverse Fourier transfer by the transfer function of the channel, here we will express the transfer function measured by the given channel mathematically in the frequency domain for the following impulse responses analysis.

Considering a multipath channel with L paths, we have following equation for the transfer function of this channel with infinite bandwidth.

$$H(f) = \sum_{l=1}^{L} a_l e^{-j2\pi f \tau_l} \tag{2.3}$$

where a_l is the amplitude of the l^{th} path, and τ_l is the time delay of the l^{th} path. By using the inverse Fourier transform, the channel impulse response is obtained from the transfer function $H(f)$ and can be written as

$$h(t) = \sum_{l=1}^{L} a_l \delta(t - \tau_l) \tag{2.4}$$

Noticed here, the channel impulse response in time domain is in the ideal case where the channel has infinite bandwidth.

The measured UWB channel spectrum is partitioned into K subbands, assuming the center frequencies of each subband are $\{f_{c_1}, f_{c_2}, f_{c_3}, ..., , f_{c_K}\}$, and the bandwidths of the subbands are equal, represented by BW_{sub}, as shown in the 2.4. The frequencies difference between the adjacent subbands are the same, represented by the Δf.

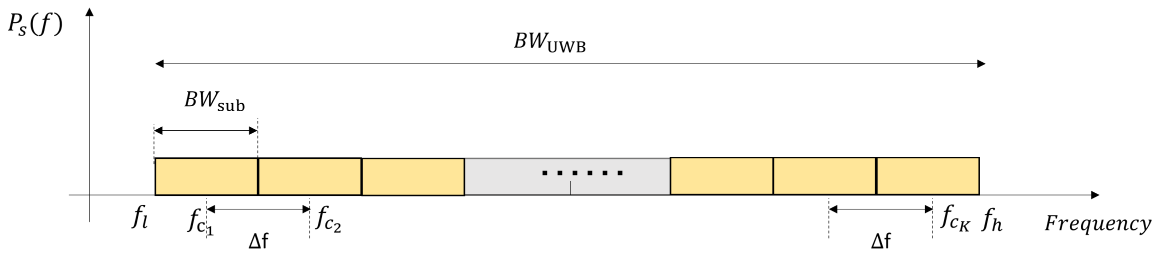

Figure 2.4: Signal Model over Frequency Domain

It is obvious there is a limitation for the center frequencies of the subbands.

$$\begin{cases} f_{c_1} - 1/2BW_{sub} \geq f_l \\ f_{c_K} + 1/2BW_{sub} \leq f_h \end{cases} \tag{2.5}$$

Design of a Multiple Subband UWB Signal

3

3.1 Overview

In this chapter, a detailed analysis of the multiple subband signal will be discussed. And the goal of this model is to find a subbands allocation scheme that has the similar performance in TOA estimation as the UWB signal.

3.2 Performance ealuation methods

In this section, two assessment methods are given for evaluating the performance of a virtual UWB signal.

3.2.1 Cramer-Rao Lower Bound

When TOA is used for range estimation, the time delay of the first arriving path is estimated. In this case, we need to evaluate the performance of the time delay estimator. The mean squared error (MSE) of an estimator θ can be written as

$$\mathrm{MSE}(\theta) = \mathrm{var}(\theta) + [\mathrm{bias}(\theta)]^2 \tag{3.1}$$

To improve the accuracy of an unbiased estimator, we need to find the smallest variance. The Cramer-Rao Lower Bound provides a lower bound of the variances [8],and is a standard way to assess the performance of constructed the virtual UWB signal on time delay estimation accuracy. A lower CRLB means a higher accuracy estimator we can reach.

For a given sample x and $\hat{\theta}$ is an unbiased scalar estimator, the CRLB can be written as [8]

$$CRLB(\theta) = \frac{1}{-E[\frac{\partial^2 \ln p(x;\theta)}{\partial \theta^2}]} \tag{3.2}$$

where the $p(x;\theta)$ is the Probability Density Function.

To calculate the CRLB, we need discretize signal. The received signal, sampled with sample time Δ seconds, can be written as

$$r[n\Delta] = a_0 s[n\Delta - \tau] + w[n\Delta] \tag{3.3}$$

Considering the samples are independent and identically distributed, the likelihood function becomes

$$
\begin{aligned}
p(r;\tau) &= \prod_{n=0}^{N-1} \frac{1}{\sqrt{2\pi\sigma^2}} exp[-\frac{1}{2\sigma^2}(r[n\Delta] - a_0 s[n\Delta - \tau])^2] \\
&= \frac{1}{(2\pi\sigma^2)^{\frac{N}{2}}} exp[-\frac{1}{2\sigma^2}\sum_{n=1}^{N}(r[n\Delta] - a_0 s[n\Delta - \tau])^2]
\end{aligned}
\tag{3.4}
$$

The first-order partial derivative of $p(r;\tau)$ with respect to τ is given by

$$
\frac{\partial \ln p(r;\tau)}{\partial \tau} = -\frac{1}{\sigma^2}\sum_{n=0}^{N-1}[(r[n\Delta] - a_0 s[n\Delta - \tau])\frac{\partial}{\partial \tau} a_0 s[n\Delta - \tau]] \tag{3.5}
$$

And the second-order partial derivative with respect to τ is

$$
\begin{aligned}
\frac{\partial^2 \ln p(r;\tau)}{\partial \tau^2} = &- \frac{a_0^2}{\sigma^2}\sum_{n=0}^{N-1}(\frac{\partial}{\partial \tau} s[n\Delta - \tau])^2 + \\
&\frac{a_0}{\sigma^2}\sum_{n=0}^{N-1}\{(r[n\Delta] - a_0 s[n\Delta - \tau])\frac{\partial^2}{\partial \tau^2} s[n\Delta - \tau]\}
\end{aligned}
\tag{3.6}
$$

The expectation of $\frac{a_0}{\sigma^2}\sum_{i=1}^{N}\{(r[n\Delta] - a_0 s[n\Delta - \tau])\frac{\partial^2}{\partial \tau^2} s[n\Delta - \tau]\}$ should be zero since the expectation of $w[n\Delta] = (r[n\Delta] - a_0 s[n\Delta - \tau])$ is zero as the source signal and the noise are independent.
So the Cramer-Rao Lower Bound now become

$$
CRLB(\tau) = \frac{1}{-E[\frac{\partial^2 \ln p(r;\tau)}{\partial \tau^2}]} = \frac{\sigma^2}{a_0^2 \sum_{n=0}^{N-1}\left[\frac{\partial}{\partial \tau} s[n\Delta - \tau]\right]^2} \tag{3.7}
$$

Equation (3.7) can also be written as

$$
CRLB(\tau) = \frac{\sigma^2}{a_0^2 \sum_{n=0}^{N-1}\left[\frac{\partial}{\partial \tau} s[n;\tau]\right]^2} \tag{3.8}
$$

Now let we assume a pulse signal $s(t)$ which is nonzero over $[0, T_s]$, and bandlimited White Gaussian noise with bandwidth B and two-sided power spectrum density $N_0/2$. Here Nyquist rate sampling is used, which means $\Delta = 1/2B$ and the noise variance is $N_0 B$.

Using $r[n]$,$s[n]$ $w[n]$ to represent the sampled received signal plus sampled noise, the sampled signal and the sampled noise, respectively, then equation (3.3) becomes

$$
r[n] = a_0 s[n\Delta - \tau] + w[n] \quad n = 0, 1, 2..., N-1 \tag{3.9}
$$

Since the pulse signal is nonzero over $[0, T_s]$, the $a_0 s\,(n\Delta - \tau_o)$ would be nonzero over $[\tau_o, T_s + \tau_o]$, where τ_o is the propagation time. Then equation (3.9) can be reduced to

$$
r[n] = \begin{cases} w[n] & 0 \le n \le n_o - 1 \\ a_0 s\,(n\Delta - \tau_o) + w[n] & n_o \le n \le n_o + M - 1 \\ w[n] & n_o + M \le n \le N - 1 \end{cases} \tag{3.10}
$$

where $n_o = \tau_o/\Delta$ ($n_o = \tau_o/\Delta$ could be approximated by an integer since Δ is so small), and M is the length of the sampled signal.

Applying (3.10) into equation (3.8),

$$\begin{aligned}
\mathrm{CRLB}\left(\tau_0\right) &= \frac{\sigma^2}{a_0^2 \sum_{n=0}^{N-1}\left(\frac{\partial s[n;\tau_0]}{\partial \tau_0}\right)^2} \\
&= \frac{\sigma^2}{a_0^2 \sum_{n=n_0}^{n_0+M-1}\left(\frac{\partial s(n\Delta-\tau_0)}{\partial \tau_0}\right)^2} \\
&= \frac{\sigma^2}{a_0^2 \sum_{n=n_0}^{n_0+M-1}\left(\left.\frac{ds(t)}{dt}\right|_{t=n\Delta-\tau_0}\right)^2} \\
&= \frac{\sigma^2}{a_0^2 \sum_{n=0}^{M-1}\left(\left.\frac{ds(t)}{dt}\right|_{t=n\Delta}\right)^2}
\end{aligned} \tag{3.11}$$

Knowing that $\Delta = 1/2B$ is small enough to approximate the sum by an integral, and $\sigma^2 = N_o B$, then

$$\mathrm{CRLB}\left(\tau_o\right) = \frac{\sigma^2}{\frac{a_0^2}{\Delta}\int_0^{T_s}\left(\frac{\partial s(t)}{\partial t}\right)^2 dt} = \frac{N_o/2}{a_0^2\int_0^{T_s}\left(\frac{\partial s(t)}{\partial t}\right)^2 dt} \tag{3.12}$$

Given that $E_s = \int_0^{T_s} s^2(t)dt$, the equation (3.12) is rewritten

$$\mathrm{CRLB}(\tau_o)\, \frac{1}{a_0^2 \frac{E_s}{N_o/2}\frac{\int_0^{T_s}\left(\frac{\partial s(t)}{\partial t}\right)^2 dt}{\int_0^{T_s} s^2(t)dt}} \tag{3.13}$$

Also the signal energy can be written as $E_s = \int_0^{T_s} s^2(t)dt = P_t \times T_s$. Then the CRLB becomes

$$\mathrm{CRLB}\left(\tau_o\right) = \frac{1}{a_0^2 \times 2\frac{P_T \times T_s}{N_0} \times B_{rms}^2}\left(\sec^2\right) \tag{3.14}$$

where B_{rms} is the RMS bandwidth

$$B_{rms} = \sqrt{\frac{\int_0^{T_s}\left(\frac{\partial s(t)}{\partial t}\right)^2 dt}{\int_0^{T_s} s^2(t)dt}} \tag{3.15}$$

Applying the Fourier transform and Parseval's theorem, RMS bandwidth becomes

$$B_{rms} = \sqrt{\frac{\int_{-\infty}^{\infty}(2\pi f)^2|S(f)|^2 df}{\int_{-\infty}^{\infty}|S(f)|^2 df}} \tag{3.16}$$

Now the CRLB of the virtual UWB signal can be calculated, as given in (2.1) and (2.2), the PSD of the signal can be given as

$$\begin{aligned} P_s(f) = |S(f)|^2 &= \sum_{k=1}^{K} |X_k(f)|^2 \\ &= \sum_{k=1}^{K} \left| X_k^{bb}\left(f - f_{a_k}\right)\right|^2 \end{aligned} \tag{3.17}$$

Substitution of equation (3.17) into (3.14), we have

$$\begin{aligned} \text{CRLB}\left(\tau_o\right) &= \frac{1}{a_0^2 \times 2\frac{P_T \times T_s}{N_0} \times B_{rms}^2} \\ &= \frac{1}{a_0^2 \times 2\frac{P_T \times T_s}{N_0} \times \frac{\int_{-\infty}^{\infty}(2\pi f)^2 |S(f)|^2 df}{\int_{-\infty}^{\infty}|S(f)|^2 df}} \\ &= \frac{1}{a_0^2 \times 2\frac{P_T \times T_s}{N_0} \times \frac{\sum_{k=1}^{K}\int_{-\infty}^{\infty}(2\pi f)^2 \left|X_k^{bb}\left(f - f_{a_k}\right)\right|^2 df}{\sum_{k=1}^{K}\int_{-\infty}^{\infty}\left|X_k^{bb}\left(f - f_{a_k}\right)\right|^2 df}} \end{aligned} \tag{3.18}$$

In this case, given a fixed transmit power P_T, transmit time period T_s and two-sided noise power $N_0/2$, in order to find a smaller CRLB, we need to find a large RMS bandwidth B_{rms} of the sparse subbands, it becomes a optimization question,

$$MAX(B_{rms}^2) = MAX\left(\frac{\sum_{k=1}^{K}\int_{-\infty}^{\infty}(2\pi f)^2 \left|X_k^{bb}\left(f - f_{a_k}\right)\right|^2 df}{\sum_{k=1}^{K}\int_{-\infty}^{\infty}\left|X_k^{bb}\left(f - f_{a_k}\right)\right|^2 df}\right) \tag{3.19}$$

From section 2, we assume that the PSD of each subband P_{sub_k} is a constant, and the power of the transmitted signal P_T is also a constant, where $P_T = \sum_{k=1}^{K} P_{sub_k}$.

Then the squared RMS bandwidth can be written as

$$\begin{aligned} B_{rms}^2 &= \frac{\sum_{k=1}^{K}\int_{-\infty}^{\infty}(2\pi f)^2 \left|X_k^{bb}\left(f - f_{a_k}\right)\right|^2 df}{\sum_{k=1}^{K}\int_{-\infty}^{\infty}\left|X_k^{bb}\left(f - f_{a_k}\right)\right|^2 df} \\ &= \frac{\frac{4\pi^2}{3}\sum_{k=1}^{K} f^3\Big|_{f_{a_k}-BW_k/2}^{f_{a_k}+BW_k/2} P_{sub_k}}{\sum_{k=1}^{K} BW_k P_{sub_k}} \\ &= \frac{\frac{4\pi^2}{3}\sum_{k=1}^{K}\left[\frac{1}{4}BW_k^2 + 3f_{a_k}^2\right] BW_k P_{sub_k}}{\sum_{k=1}^{K} BW_k P_{sub_k}} \end{aligned} \tag{3.20}$$

Assuming every subband signal has the same fixed PSD and bandwidth BW, the squared RMS bandwidth now becomes

$$B_{rms}^2 = \frac{4\pi^2}{3}\sum_{k=1}^{K}\left[\frac{1}{4}BW^2 + 3f_{a_k}^2\right] \tag{3.21}$$

There are still some constrains.

1. The virtual bandwidth is BW_{UWB},

$$f_{a_K} - f_{a_1} + \frac{1}{2} \times (BW_1 + BW_K) = BW_{UWB} \tag{3.22}$$

2. There is no overlap between subbands

$$f_{a_{n+1}} - f_{a_n} \geq \frac{1}{2} \times (BW_n + BW_{n+1}), n = 0, 1, 2...K - 1 \tag{3.23}$$

It's obvious that the CRLB is influenced by the number of subbands, their bandwidths, the PSDs of the subband signals, and also the locations of the subbands.

3.2.2 Squared error of the auto-correlation

At the receiver, correlation in the time domain is widely used for time delay estimation. The correlation function measures the similarity between two signals for all possible delays, and the peak of the correlation function occurs at the delay with the best similarity between the two signals, therefore, it is important to find the peak of the correlation function precisely. For that purpose, the correlation should have a distinct and outstanding peak. And in practice the cross-correlation of the received signal and an ideal replica of the transmitted signal will be used to estimate the delay, but here we will use auto-correlation of the virtual signal to simulate and find whether it has a distinct peak.

The auto-correlation of the sparse subbands signal can be written as the sum of the auto-correlations of the baseband subband signals [9], and the detailed derivation is shown in Appendix A.

In this case, the auto-correlation of the virtual signal given in (2.2) is

$$\begin{aligned} R_x(\tau) &= \sum_{k=1}^{K} R_{x_k}(\tau) \\ &= \sum_{k=1}^{K} R_{x_k^{bb}}(\tau) e^{j2\pi f_{a_k} \tau} \end{aligned} \tag{3.24}$$

where $R_{x_k^{bb}}(\tau)$ is the auto-correlation of each of the baseband subband signals.

In order to find a correlation with a distinct and outstanding peak, we will use the ideal auto-correlation of a signal which has the constant PSD P_{ideal} spanning the full bandwidth BW_{UWB} as benchmark, where the correlation function will only show one peak at $\tau = 0$ point. Then the difference between the correlation of the constructed virtual signal and benchmark will be determined to evaluate the performance of the virtual signal.

The auto-correlation of the full UWB channel can be written as

$$
\begin{aligned}
R_{ideal}(\tau) &= \mathcal{F}^{-1}\left\{|X_{ideal}(f)|^2\right\} \\
&= \int_{-\infty}^{\infty} P_{ideal} e^{j2\pi f\tau} df \\
&= \frac{P_{ideal}}{j2\pi\tau}\left(e^{j\pi BW_{UWB}\tau} - e^{-j\pi BW_{UWB}\tau}\right) \\
&= \frac{P_{ideal}}{\pi\tau}\sin \pi BW_{UWB}\tau \\
&= P_{ideal} BW_{UWB} \operatorname{sinc} BW_{UWB}\tau
\end{aligned} \tag{3.25}
$$

Assuming there are K subbands, BW is the bandwidths of the subbands, and the PSD of each subband is

$$
P_{sub} = \frac{p_{ideal} \times BW_{UWB}}{K \times BW} \tag{3.26}
$$

where the P_{ideal} is the PSD of the full UWB signal.

Let us introduce α as the fraction of occupied bandwidth by the subbands in the virtual UWB signal where

$$
\alpha = \frac{BW}{BW_{UWB}} \tag{3.27}
$$

Thus the auto-correlation function of the signals consisting of sparse subbands is

$$
\begin{aligned}
R_x(\tau) &= \frac{P_{sub}}{\pi\tau}(\sin \pi BW\tau)\sum_{i=1}^{K} e^{j2\pi f_{a_i}\tau} \\
&= P_{sub}BW(\operatorname{sinc} BW\tau)\sum_{i=1}^{K} e^{j2\pi f_{a_i}\tau}
\end{aligned} \tag{3.28}
$$

To calculate the squared error, summing up the squared differences at different time point is the most intuitive and obvious way, therefore the signal is sampled with time period Δ, then the squared error can be written as

$$
\begin{aligned}
E &= \sum_N |R_x(n\Delta) - R_{ideal}(n\Delta)|^2 \\
&= \sum_N |P_{sub}BW(\operatorname{sinc} BWn\Delta)\sum_{k=1}^{K}(e^{j2\pi f_{a_k}n\Delta}) - p_{ideal}BW_{UWB}\operatorname{sinc} BW_{UWB}n\Delta|^2 \\
&= \sum_N [(P_{sub}BW(\operatorname{sinc} BWn\Delta)\sum_{k=1}^{K}(\cos 2\pi f_{a_k}n\Delta) - KP_{sub}BW \operatorname{sinc}\frac{BWn\Delta}{\alpha})^2 \\
&+ (P_{sub}BW(\operatorname{sinc} BWn\Delta)\sum_{k=1}^{K}(\sin 2\pi f_{a_k}n\Delta))^2]
\end{aligned} \tag{3.29}
$$

3.3 Optimization methods

In the previous section, the squared error has been given. In this section the goal is to find the minimum value of the squared error.

3.3.1 Newton's method

Newton's method is introduced here to find the (local) minimum of a twice-differentiable function. First, we will approximate the objective function with a second-order Taylor expansion of the objective function.

The Taylor expansion for the objective function $f(x)$ at x_k can be written as

$$f\left(x_k + \Delta x\right) \approx f\left(x_k\right) + \nabla f\left(x_k\right)\Delta x + \frac{1}{2}\nabla^2 f\left(x_k\right)(\Delta x)^2 \tag{3.30}$$

Next, take the partial derivatives of each side with respect to Δx, we have

$$\nabla f\left(x_k + \Delta x\right) \approx \nabla f\left(x_k\right) + \nabla^2 f\left(x_k\right)\Delta x \tag{3.31}$$

And then we let the $\nabla f\left(x_k + \Delta x\right) = 0$ to reach the minimum of $f\left(x_k + \Delta x\right)$, the Newton step becomes

$$\Delta x = -\frac{\nabla f}{\nabla^2 f} \tag{3.32}$$

And $\nabla f(x)$ is the gradient of the function. $\nabla^2 f$ is the Hessian, which consists of the second partial derivatives of the objective function with respect to each of the variables. The recurrence relation of variables can be written as

$$x_{k+1} = x_k - H^{-1}\left(x_k\right)\nabla f\left(x_k\right) \tag{3.33}$$

In this case, once we have an initial start value x_0, then apply iteration through Newton's method, and set a suitable threshold for stopping the iteration, we can obtain the x_k where the minimum of objective function is reached.

3.3.2 Application of Newton's method

In order to meet the constrain given in (3.22), there will be two fixed subbands centered at the edges of the virtual bandwidth. Therefore, there actually are $K-2$ independent variables. In order to simplify the calculation, we assume the fixed two subbands are the $K-1_{th}$ subband and K_{th} subband and their center frequencies are $f_{a_{K-1}}$, f_{a_K}, therefore, the other center frequencies of baseband signals are represented by $\boldsymbol{f_a} = [f_{a_1}, f_{a_2}, ..., f_{a_{K-2}}]^T$. Here the squared error can be seen as sum function of N time points, which means it can be written as $E = \sum_N y_n^2$ and we have

$$\begin{aligned} y_n &= |R_x(n\Delta) - R_{ideal}(n\Delta)|_1 \\ &= ((P_{sub}BW(\operatorname{sinc} BWn\Delta)\sum_{k=1}^{K}(\cos 2\pi f_{a_k}n\Delta) - KP_{sub}BW \operatorname{sinc}\frac{BWn\Delta}{\alpha})^2 \\ &+ (P_{sub}BW(\operatorname{sinc} BWn\Delta)\sum_{k=1}^{K}(\sin 2\pi f_{a_k}n\Delta))^2)^{\frac{1}{2}} \end{aligned} \tag{3.34}$$

In order to minimise the squared error $E = \sum_N y_n^2$, we apply the Newton's method. The Jacobian matrix is introduced here which consisting of the first partial derivatives of the objective function with respect to each of the variables. And it can be expressed as

$$\boldsymbol{J} = \begin{bmatrix} \frac{\partial y_1}{\partial f_{a_1}} & \cdots & \frac{\partial y_1}{\partial f_{a_{K-2}}} \\ \vdots & \ddots & \vdots \\ \frac{\partial y_N}{\partial f_{a_1}} & \cdots & \frac{\partial y_N}{\partial f_{a_{K-2}}} \end{bmatrix} \tag{3.35}$$

The first derivative of y_i with respect to any $f_{a_i}(i = 1, 2, ..., K-2)$ is

$$\begin{aligned} \frac{\partial y_n}{\partial f_{a_i}} = &-((P_{sub}BW(\operatorname{sinc} BWn\Delta)\sum_{k=1}^{K}(\cos 2\pi f_{a_k} n\Delta) - KP_{sub}BW \operatorname{sinc} \frac{BWn\Delta}{\alpha})^2 \\ &+ (P_{sub}BW(\operatorname{sinc} BWn\Delta)\sum_{k=1}^{K}(\sin 2\pi f_{a_k} n\Delta))^2)^{-\frac{1}{2}} \times \\ &([P_{sub}BW(\operatorname{sinc} BWn\Delta)\sum_{k=1, k\neq i}(\cos 2\pi f_{a_k} n\Delta) \\ &- KP_{sub}BW \operatorname{sinc} \frac{BWn\Delta}{\alpha}](2\pi n\Delta P_{sub}BW)(\sin \pi BWn\Delta)\sin 2\pi f_{a_i} n\Delta \\ &+ KP_{sub}BW \operatorname{sinc} \frac{BWn\Delta}{\alpha} \sum_{k=1, k\neq i}(sin 2\pi f_{a_k} n\Delta)) \end{aligned} \tag{3.36}$$

Also the Hessian is

$$\boldsymbol{H} = \begin{bmatrix} \frac{\partial^2 y_1}{\partial f_{a_1}^2} & \frac{\partial^2 y_2}{\partial f_{a_1}\partial f_{a_2}} & \cdots & \frac{\partial^2 y_2}{\partial f_{a_1}\partial f_{a_{K-2}}} \\ \frac{\partial^2 y_3}{\partial f_{a_2}\partial f_{a_1}} & \frac{\partial^2 y_2}{\partial f_{a_2}^2} & \cdots & \frac{\partial^2 y_3}{\partial f_{a_2}\partial f_{a_{K-2}}} \\ \vdots & \vdots & \ddots & \vdots \\ \frac{\partial^2 y_N}{\partial f_{a_{K-2}}\partial f_{a_1}} & \frac{\partial^2 y_N}{\partial f_{a_{K-21}}\partial f_{a_2}} & \cdots & \frac{\partial^2 y_N}{\partial f_{a_{K-2}}^2} \end{bmatrix} \tag{3.37}$$

As given in (3.33), in this case, it becomes

$$\boldsymbol{f_{a_i}}^{(n+1)} = \boldsymbol{f_{a_i}}^{(n)} - \boldsymbol{H}^{-1}\boldsymbol{g} \tag{3.38}$$

where $\boldsymbol{g}$ denotes the gradient vector of $\boldsymbol{E}$ and $\boldsymbol{H}$ denotes the Hessian matrix of E. Therefore, the gradient vector $\boldsymbol{g}$ can be also written as $2\boldsymbol{J_E}^T\boldsymbol{E}$, where $\mathbf{J_E}$ is the Jacobian matrix, so the recurrence relation can be written as

$$\boldsymbol{f_{a_i}}^{(n+1)} = \boldsymbol{f_{a_i}}^{(n)} - 2\boldsymbol{H}^{-1}\boldsymbol{J_E}^T\boldsymbol{E} \tag{3.39}$$

Therefore for every step, we will update our $\boldsymbol{f_{a_i}}$ until the change of E becomes smaller than a threshold. In this case, the threshold is set to 0.001, which means that if a new f_{a_i} is updated and the change of error of the auto-correlation does not exceed 0.00001, the minimum of the function will be found.

Note here that in order to simplify the calculations, Gauss Newton's method is also introduced. In this case, we do not need to calculate the Hessian matrix, but an estimate will be used $\mathbf{H} \approx 2{\mathbf{J}_{\mathrm{E}}}^{\top}\mathbf{J}_{\mathbf{E}}$. And the recurrence relation becomes

$$\boldsymbol{f_{a_i}}^{(n+1)} = \boldsymbol{f_{a_i}}^{(n)} - 2{\mathbf{J}_{\mathbf{E}}}^{\top}{\mathbf{J}_{\mathbf{E}}}^{-1}{\boldsymbol{J_E}}^{T}\boldsymbol{E} \tag{3.40}$$

In this case, the locations of the subbands when we have a minimum error of autocorrelation can be calculated.

Results for Different Multiple Subbands UWB Signals

4

In this chapter, simulations of the assessment methods given in Chapter 3 are discussed, and also the results of optimization of the auto-correlation error are shown.

4.1 Results for the assessment of constructed virtual UWB signals

In the following simulation, we use the virtual bandwidth which is 1 GHZ and the subband bandwidth 50 MHz. Assuming we have K subbands, and the PSD of subband signal is 1/K.

4.1.1 Results of Cramer-Rao Lower Bound

As given in Chapter 3, CRLB can give the lowest bound of the unbiased estimator. When the constructed virtual signals are used for the delay estimation, we will see how the CRLB change when different subbands are chosen.

Several sparse subbband signals are introduced as examples, and the change of the CRLB given in (3.14) versus location of subbands will be given.

4.1.1.1 Case 1: 3 Subbands

Considering there are three sparse subband signals, and two of the subband signals' locations are fixed at the edge of the virtual band, the third signal location f_{a_2} will shift from the left edge to the right edge based on a given step, as shown in 4.1.

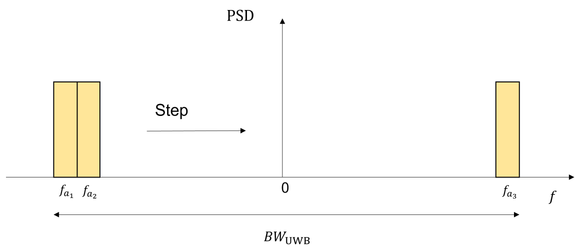

Figure 4.1: Diagram: Three Sparse Subband Signals Case

And the frequency step is 10 MHz in this case. Based on (3.18), the CRLB is shown in 4.2

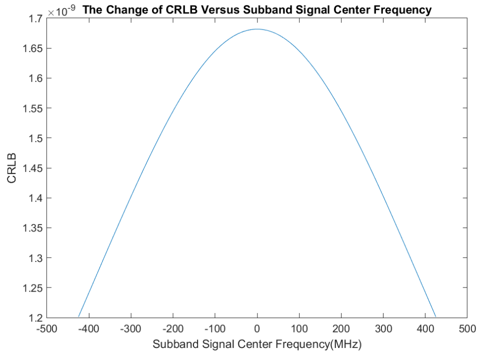

Figure 4.2: The change of CRLB versus subband center frequency with 3 subbands

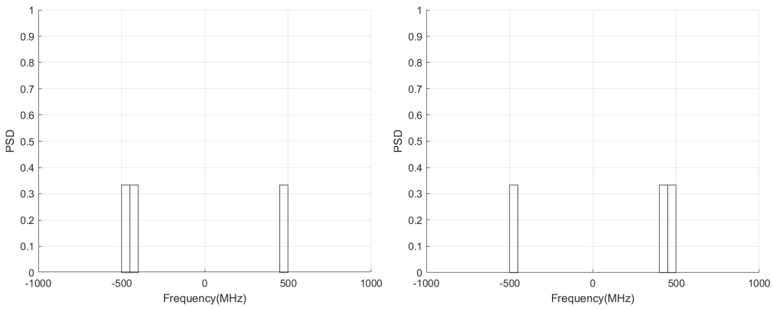

Figure 4.3: Two subband signals allocation with lowest CRLB when the number of subband is 3

As shown in figure 4.2, it is obvious that the CRLB is a convex function. To find the lowest CRLB, the third subband should be at the edges of the subbands as shown in figure 4.3. As given in (3.21), when the bandwidth of subbands are fixed, then the squared center frequency should be larger to have a lager RMS bandwidth, leading to the smaller CRLB.

To sum up, the lower CRLB can be achieved when the subband signals are centered at the edges of the virtual band. Just like [10] concludes, the more the power of the signal is concentrated at the edge of the band, the lower CRLB we can have. But what should be mentioned here is that this will cause more ambiguity errors which will be discussed later.

4.1.1.2 Case 2: 4 Subbands

Considering the case with 4 subband signals, fixing three subband signals at the edge of the virtual band for simplifying the calculation, and the fourth subband shift from left side to the right side inside the virtual bandwidth. Based on (3.18),the CRLB is calculate. The result is shown in 4.4

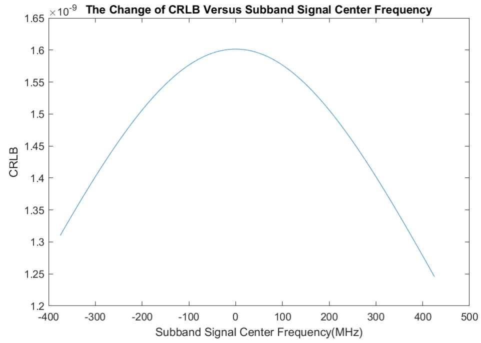

Figure 4.4: The change of CRLB versus subband Center Frequency with 4 subbands)

When we have the lowest CRLB, the allocation of the subbands is

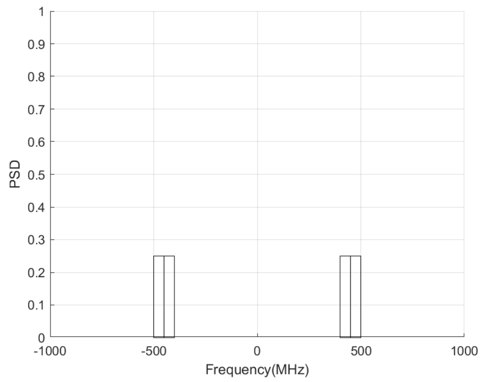

Figure 4.5: Subbands allocation with lowest CRLB

As shown in figure 4.4 and figure 4.5, the CRLB function with respect to the location of the subbands is still a convex function. Therefore, the similar result is found as in the three subbands case. In order to achieve the lowest CRLB, the central frequency of the subbands should be centered as close as possible to the edge of the virtual band, and a symmetric spectrum reaches.

4.1.2 Squared error of the auto-correlation

In this section, we will use the three subbands case as an example. The two subband signals are fixed at the two edges of the virtual UWB band, Assume virtual bandwidth is 1 GHz, and the bandwidth of the subbands is 50 MHz. So if the third subband is put at the middle between the fixed two subbands as shown in 4.6

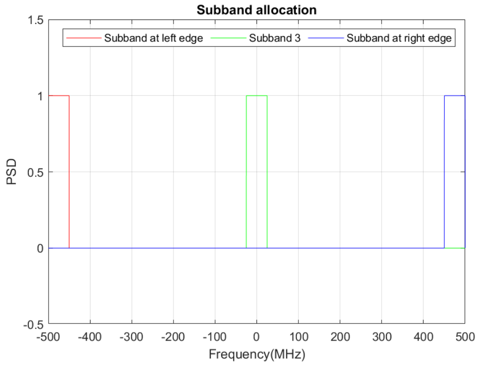

Figure 4.6: Subband allocation

The real auto-correlation, imaginary auto-correlation of each subband and also the auto-correlation of the constructed virtual signal are shown in 4.7 and 4.8.

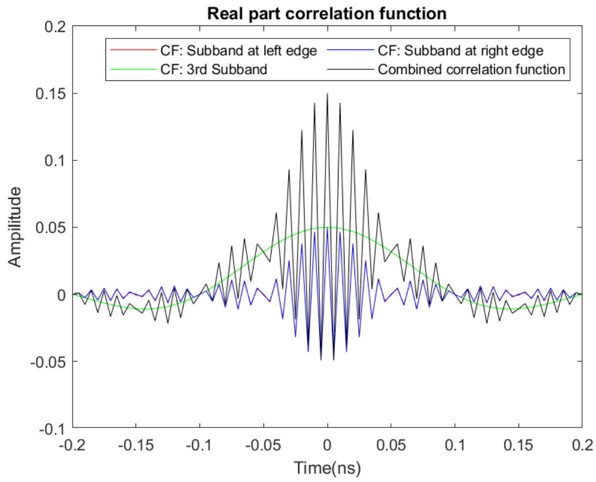

Figure 4.7: Real part correlation function of different subbands and combined subband

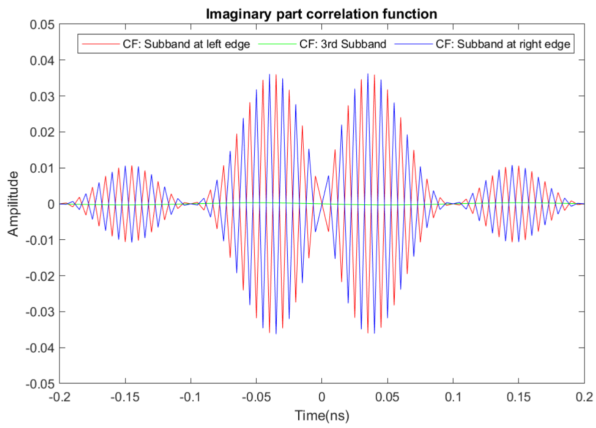

Figure 4.8: Imaginary part correlation function of different subbands

From figure 4.7, the correlation function of combined virtual signal has multiple peaks, which poses a serious challenge in the time of arrival estimation. Here we use the minimum squared error to measure the auto-correlation performance. Assuming there is a UWB signal spanned over the virtual bandwidth, and the transmit power of it is the same as the virtual UWB signal, then both auto-correlation functions are calculated. We measure the squared difference between two functions at different time points, then sum them up to have the squared error. From figure 4.9, we see that there is a large difference between two correlations.

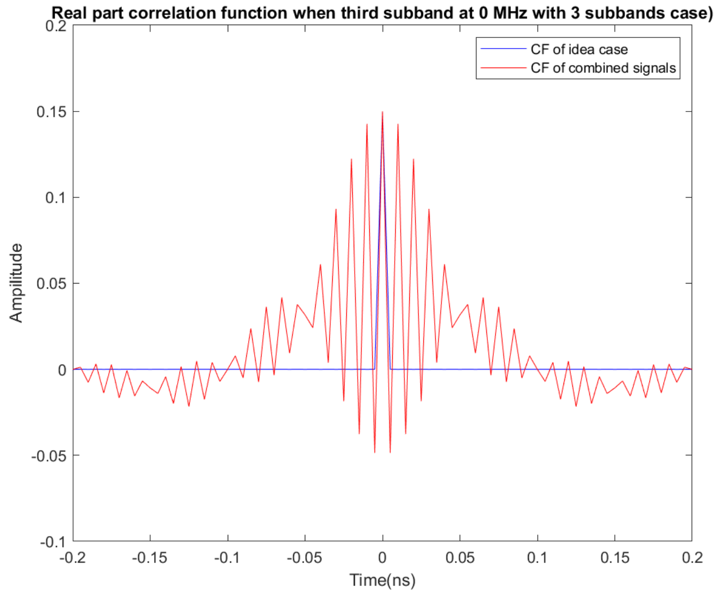

Figure 4.9: Real part correlation Function of combined UWB signal and the ideal virtual UWB signal

The squared error between these two curves can be seen as the assessment method to measure the similarity of these two curves, leading to measure the performance of the auto-correlation of combined signal.

4.1.2.1 Optimization method

In order to minimise the squared error given in (3.29), the Newton method and the Gauss Newton method are used here.

Here we still use 3 subband case as the example, two of them are fixed at the edges of the virtual band, the third subband shifts from left edge to the right edge based on the step.

Same parameters we use to calculate the CRLB are given, the results in 4.1 show a weird result that the optimal center frequency of the third subband is always close to the starting point of the algorithm, it seems wherever we start the algorithm, the optimal value will stop at a local minimum value.

Start frequency(MHz)	400	300	200	100	0
End frequency (MHz)	398	299	200	98	75

Table 4.1: The results of Newton's method on squared error

To figure out this problem, we calculate the first derivative of the squared error function directly, the result is shown in 4.10 .

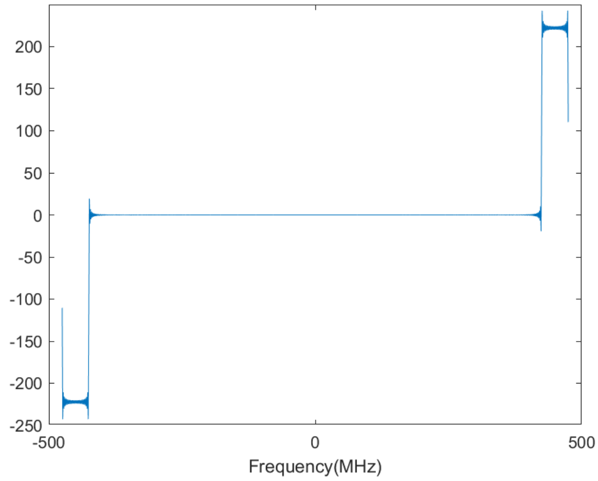

Figure 4.10: Change of derivative versus center frequency

As shown in the 4.10, actually the derivative repeatedly crosses the zero point, which means there are a lot local minimum point, and actually it is hard to find a optimal value. Then we look at the squared error in 4.11 directly.

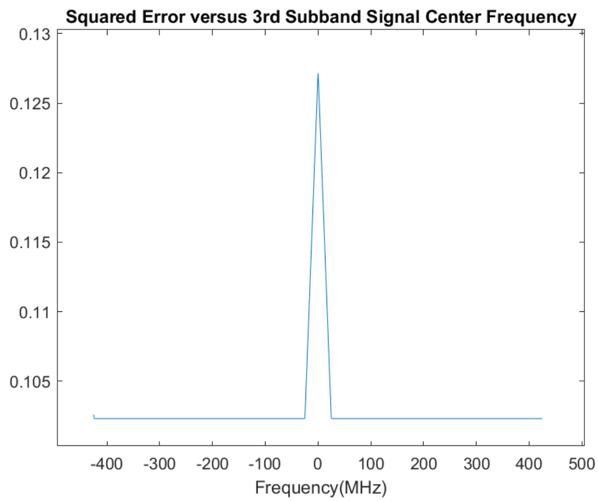

Figure 4.11: Squared error

We can find that actually the squared error does not change too much when the third subband shifts from left side to the right side. Thus the squared error of the auto-correlation does not make much sense since most subband allocation schemes show similar error. In other words, the method we proposed for evaluating the auto-correlation is not good enough to judge the quality of the performance. It is determined that if the third subband is not close to the center frequency, we can have the combined virtual UWB signals with same performance on auto-correlation.

Frequency Dependence of the Channel Impulse Response

5

In this chapter, a detailed analysis of the frequency dependence of the channel impulse response will be discussed. The goal of this analysis is to find the frequency relationship of the CIR of subbands extracted from an UWB channel.

5.1 Channel model

In Chapter 2, we already presented the mathematical expressions of the transfer function and channel impulse response of the channel. Here, we will derive the the mathematical expressions for the transfer function and the frequency response of the subbands.

In order to obtain the subbands, a window function is introduced to truncate the full UWB spectrum, which also reduce the spectrum leakage caused by the finite bandwidth we have.

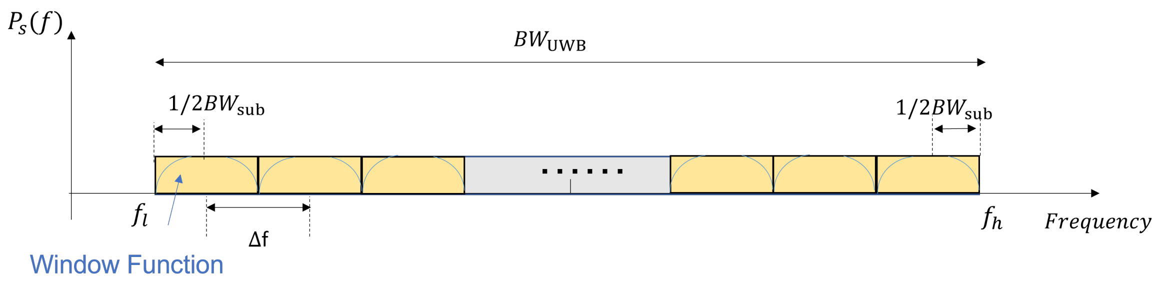

Figure 5.1: Windowed channel response model in the frequency domain

As shown in figure 5.1, window functions centered at $\{f_{c_1}, f_{c_2}, f_{c_3}, ..., , f_{c_K}\}$ are used to create the subband transfer function.

$$H_k(f) = H(f)W_k(f) \tag{5.1}$$

where $W_k(f) = W(f - f_{c_k})$ is the window function centered at f_{c_k} with bandwidth BW_{sub}. In the time domain, the window function is obtained by the inverse Fourier transform and can be written as

$$w_k(t) = \mathcal{F}^{-1}\{W_k(f)\} = w(t)e^{j2\pi f_{c_k} t} \tag{5.2}$$

where $w(t)$ is the baseband window function in the time domain. Then the subband CIR is obtained by taking the inverse Fourier transform of the windowed subband signal. Now, the CIR is found as

$$h_k(t) = \mathcal{F}^{-1}\{H_k(f)\} = \sum_{l=1}^{L} a_l \delta(t - \tau_l) * w_k(t) \tag{5.3}$$

And from (5.2) and (5.3), the CIR can be represented by

$$h_k(t) = e^{j2\pi f_{c_k} t} \sum_{l=1}^{L} a_l e^{-j2\pi f_{c_k} \tau_l} w(t - \tau_l) \tag{5.4}$$

To simplify the calculations, the subband signals are moved to baseband, and the baseband subband CIRs can be represented as

$$h_{bbk}(t) = \sum_{l=1}^{L} a_l e^{-j2\pi f_{c_k} \tau_l} w(t - \tau_l) \tag{5.5}$$

where the term $2\pi f_{c_k} \tau_l$ is the phase of the l_{th} path. When using a matrix representation of the basband subband CIRs, we get

$$h_{bbk}(t) = \begin{bmatrix} a_1 e^{-j2\pi f_{c_k} \tau_1} w(t - \tau_1) \\ a_2 e^{-j2\pi f_{c_k} \tau_2} w(t - \tau_2) \\ \vdots \\ \vdots \\ a_l e^{-j2\pi f_{c_k} \tau_l} w(t - \tau_L) \end{bmatrix}^T \begin{bmatrix} 1 \\ 1 \\ \vdots \\ \vdots \\ 1 \end{bmatrix} \tag{5.6}$$

Now we introduce a variable Δf which indicates the frequency distance between adjacent center frequencies. The number of subbands can be influenced by changing Δf. If the bandwidth of the subbands is fixed, there might be gaps between adjacent subbands when Δf increases. Similarly, there might be overlaps between adjacent subbands when Δf is quite small. The formula of Δf is given as

$$\Delta f = f_{c_{k+1}} - f_{c_k} \tag{5.7}$$

In this case, by substituting equation (5.7) into equation (5.5), the adjacent subband of the k^{th} band $k + 1^{th}$ band can be written as

$$\begin{aligned} h_{bb(k+1)}(t) &= \sum_{l=1}^{L} a_l e^{-j2\pi f_{c_{k+1}} \tau_l} w(t - \tau_l) \\ &= \sum_{l=1}^{L} a_l e^{-j2\pi f_{c_k} \tau_l} w(t - \tau_l) e^{-j2\pi \Delta f \tau_l} \end{aligned} \tag{5.8}$$

This case can be written in matrix form as:

$$h_{bb(k+1)}(t) = \begin{bmatrix} a_1 e^{-j2\pi f_{c_k} \tau_1} w(t - \tau_1) \\ a_2 e^{-j2\pi f_{c_k} \tau_2} w(t - \tau_2) \\ \vdots \\ \vdots \\ a_l e^{-j2\pi f_{c_k} \tau_l} w(t - \tau_L) \end{bmatrix}^T \begin{bmatrix} e^{-j2\pi \Delta f \tau_1} \\ e^{-j2\pi \Delta f \tau_2} \\ \vdots \\ \vdots \\ e^{-j2\pi \Delta f \tau_L} \end{bmatrix} \tag{5.9}$$

Comparing equations 5.6 and 5.9, an interesting behavior is found. Adjacent subbands only show a phase rotation $e^{j2\pi\Delta f\tau_l}$ in the l_{th} path related to time delay τ_l and frequency separation Δf, and this phase rotation matrix $\phi_{rotation}$ is given as

$$\phi_{rotation} = \begin{bmatrix} e^{-j2\pi\Delta f\tau_1} \\ e^{-j2\pi\Delta f\tau_2} \\ \vdots \\ \vdots \\ e^{-j2\pi\Delta f\tau_L} \end{bmatrix} \tag{5.10}$$

5.2 Window function

For processing the subband channel, the frequency domain measurements need to be truncated to subbands with bandwidth BW_{sub} by multiplying the full band response with a window function with respective center frequency and bandwidth. The most serious impact after windowing is the inevitable spectrum leakage and the main reason for spectrum leakage is that when the spectrum of the window function is infinitely long and the signal is convolved, the main lobe and the side lobe are superimposed, so the smaller the energy of the side lobe, the smaller the influence of spectrum leakage.

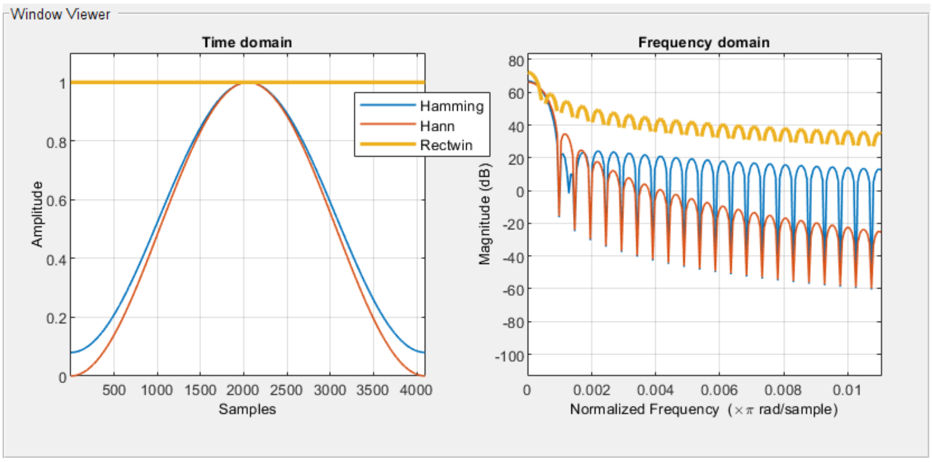

Figure 5.2: Hann, Hamming and Rectangular Windows

In our model, we focus on the covariance of the CIRs of subbands at different time delays, which means the main lobe should be as narrow as possible, so as to have a more accurate time resolution. Thus, a suitable window function which has narrow main lobe and superior side lobes should be found. Let us consider the most popular window functions Hann, Hamming, rectangular windows, the spectrum in time domain and frequency domain are shown in 5.2

When we compare these three window functions, we find that the rectangular window has the narrowest main lobe but the largest amplitude of side lobes. The other two window functions have wider main lobes but lower side lobes. None of them has a narrow main lobe and lower side lobes at the same time. Therefore, the Tukey window is considered since it is a window that can be seen as a trade-off between the Hamming and rectangular windows. The Tukey window is expressed by following equations

$$\begin{cases} w[n] = \frac{1}{2}\left[1 - \cos\left(\frac{2\pi n}{\alpha N}\right)\right], & 0 \leq n < \frac{\alpha N}{2} \\ w[n] = 1, & \frac{\alpha N}{2} \leq n \leq \frac{N}{2} \\ w[N-n] = w[n], & 0 \leq n \leq \frac{N}{2} \end{cases} \tag{5.11}$$

As shown in figure 5.3, by choosing a smaller cosine fraction α , the ”flat” part will become larger, and after inverse Fourier transform, the main time lobe becomes narrower, and the side lobes roll-off rate becomes worse and side lobe height becomes lower.

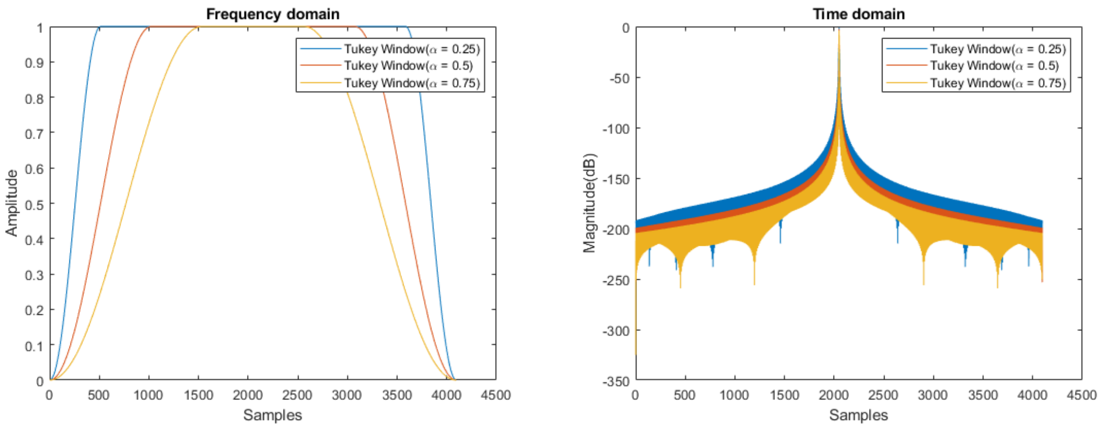

Figure 5.3: Tukey Window with 0.25,0.5,0.75

In order to remove the noise and residual signal when processing the received signal, we introduce a noise threshold that the spectrum below this threshold is considered to be full of noise. And here the noise threshold is set at 30 dB below the strongest multipath component (MPC) which is around 0 dB, therefore we mainly focus on the spectrum exceeding -30 dB in time domain. As shown in figure 5.4, the main lobe is wider below -30 dB and more noise will be involved when the cosine fraction α is small.

In practice, we need to find the trade-off between narrower main lobe and superior side lobe roll-off, narrower means a smaller α is needed, and superior side lobe roll-off means a larger α is needed, so we have a compromise here and choose the middle value $\alpha = 0.5$ to balance the trade-off.

5.3 Frequency dependence

In order to measure the frequency dependence of the channel impulse responses of the subbands, the covariance function between adjacent subbands in baseband is determined.

From equations 5.6 and 5.9, the CIRs of adjacent baseband signals only show a phase difference in multipath components, which depends on Δf and τ_l. In this case, in order to have the covariance of two adjacent bands, the first step is to compensate

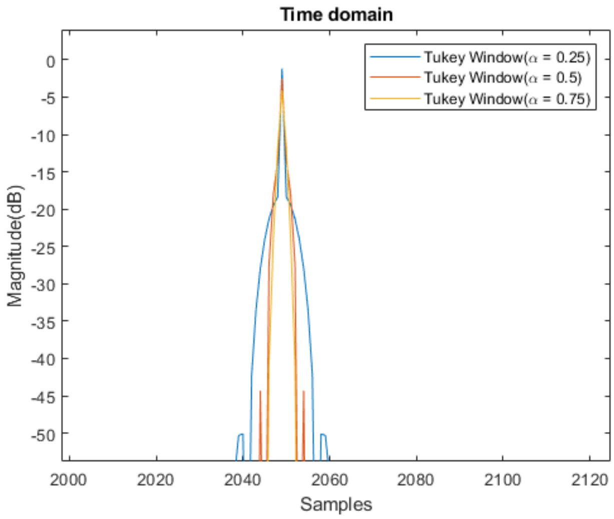

Figure 5.4: Tukey Window with 0.25,0.5,0.75

the phase rotation. In TOA estimation, accurate time delay estimation leads to the accurate positioning result, especially the time delay of the direct path. Therefore, the CIRs of subband channels at different time delays for different Δf is what really matters, and whether the change of Δf has a big impact on the CIRs of the subband signals at particular time delays.

Given K subbands and $k = 1, 2, ..., K$, then the covariance function with respect to time delay is defined as

$$R(\Delta f, \tau) = \frac{\sum_{k=1}^{k=K-1} h_{bbk}(\tau)(h_{bb(k+1)}(\tau)e^{j2\pi\Delta f\tau})^*}{K-1} \tag{5.12}$$

where the number of subbands K is given by

$$K = \lceil \frac{BW - BW_{sub}}{\Delta f} \rceil \tag{5.13}$$

In this formula, the phase rotation is compensated for each time delay. We calculate the product of the channel impulse responses of each adjacent subband channel, where the conjugation operation and phase compensation are used to eliminate the imaginary part of the product. Since we have K subband channels, we end up with K-1 products, and the average of these products is the covariance we need. Since the number of subbands will change when different subbands bandwidths and Δf are chosen, we use the maximum K as default.

Notice that here the covariance is taken over all the subbands at the the same delay time. Its normalized value can be written as

$$\begin{aligned}\rho_1(\Delta f; \tau) &= \frac{R(\Delta f, \tau)}{|R(\Delta f, \tau)|} \\ &= \frac{\sum_{k=1}^{k=K-1} h_{bbk}(\tau)(h_{bb(k+1)}(\tau)e^{j2\pi\Delta f\tau})^*}{\sum_{k=1}^{k=K-1} |h_{bbk}(\tau)||h_{bbk+1}(\tau)|}\end{aligned} \tag{5.14}$$

The normalized value ranges from 1 to -1. When it equals to 1, it means the subband CIRs are totally correlated and if it equals to -1, it means the subband CIRs are completely uncorrelated. For a given set of subbands, the frequency dependence is well characterized by the value of the covariance $\rho(0;\tau)$, where all the subbands are the same and the covariance is constant 1. Here we use 0.5 as the threshold value to determine whether the subband CIRs at delay τ is correlated, if the covariance is greater than 0.5, the subband CIRs at delay τ are treated as correlated, and conversely, if the covariance is less than 0.5, the subband CIRs at delay τ are treated as uncorrelated.

And we also give a modified normalized value,

$$\rho_2(\Delta f;\tau) = \sum_{k=1}^{k=K-1} \frac{h_{bbk}(\tau)(h_{bb(k+1)}(\tau)e^{j2\pi\Delta f\tau})^*}{|h_{bbk}(\tau)||h_{bbk+1}(\tau)|}/(K-1) \tag{5.15}$$

Results on the Frequency Dependence of the CIR

6

In this chapter, the method introduced last chapter will be validated with measured CIRs. From the simulated results, more analysis will be given for different UWB CIRs. Additionally, the frequency dependence of the direct path and reflected paths are discussed.

6.1 Simulation setup

In the last chapter, we proposed two methods based on the covariance given by (5.14) and (5.15) to determine the frequency dependence of the impulse response. The following question is to figure out how the covariance depends on the frequency separation Δf at different time delay τ, thus we need to choose a time delay τ to calculate the covariance.

In the following simulation, we take the impulse response of the UWB signal as the reference to pick up the time delay to measure the covariance.

For the proposed covariance methods (5.14) and (5.15), notice there are a common item $h_{bbk}(\tau)(h_{bb(k+1)}(\tau)e^{j2\pi\Delta f\tau})^*$ changes with Δf in the nominator and the denominator can not be affected by the imaginary part caused by the Δf, then we focus on the nominator.

Looking at the key calculation in the nominator,

$$
\begin{aligned}
&h_{bbk}(\tau)(h_{bb(k+1)}(\tau)e^{j2\pi\Delta f\tau})^* \\
&=\sum_{l_1=1}^{L} a_{l_1}e^{-j2\pi f_{c_k}\tau_{l_1}}w(\tau-\tau_{l_1})(\sum_{l_2=1}^{L} a_{l_2}e^{-j2\pi f_{c_k}\tau_{l_2}}w(\tau-\tau_{l_2})e^{-j2\pi\Delta f\tau_{l_2}}e^{j2\pi\Delta f\tau})^* \\
&=\sum_{l_1=1}^{L}\sum_{l_2=1}^{L} a_{l_1}a_{l_2}e^{-j2\pi f_{c_k}(\tau_{l_1}-\tau_{l_2})}w(\tau-\tau_{l_1})w(\tau-\tau_{l_2})e^{-j2\pi\Delta f(\tau-\tau_{l_2})}
\end{aligned}
\tag{6.1}
$$

where L is the number of the paths in the subbands and l_1, l_2 represent the paths in two adjacent subbands.

Based on this equation, the correlation of the subbands will be influenced by the change of Δf and τ. There is a main interference item $e^{-j2\pi\Delta f(\tau-\tau_{l_2})}$. The more paths in the channel, more interference will be introduced. And the appearance of this interference is because that we can not fully compensate for the phase rotation. In case that the impulse response shows multiple paths in the calculation process when we obtain CIRs by using inverse Fourier Transform, we can not separate the paths in time domain. This means CIRs can not be mathematically expressed by the sum of different paths in practice, therefore, the phase rotation shown in equation (5.10) can not be fully compensated for each path, but through the the window functions product $w(\tau - \tau_{l_1})w(\tau - \tau_{l_2})$, if there is enough time difference between two paths in time domain, large part of the impacts caused by multipath can be reduced since the window function takes a maximum value 1 at $w(0)$ and then gradually decreases to 0 on both sides, so if there is enough gap between the multiple paths, these paths will be filtered out by the low magnitude of window function and we can still have reliable results.

Here we will validate how this method performs in the ideal case which only have one path and also the case with multiple paths.

6.2 Simulation results of artificially generated UWB channels

In this section, we will validate the proposed methods. Some ideal UWB CIRs which only have several arrival paths and noise are given. Based on these channels, the frequency dependence of the subbands impulses response at specific time delays will be determined and analysed. All the artificial generated UWB channels here have the same bandwidth $5GHz$ with a center frequency 7.5 GHz as the measured one.

Considering the CIR with the signal path at 400 ns, as shown in figure 6.1. The subbands CIRs are shown in right side, only three subbands CIRs are shown here as an example.

To obtain these subbands, we first calculate the maximum number K of subbands we can have based on a $\Delta f = 60MHz$ by using equation (5.13), next, we can have evenly distributed K frequencies from 5 to 10 GHz based on the interval of 60 MHz, and then using the K Tukey Windows centered at K frequencies with $\alpha = 0.5$ and $BW_{sub} = 60MHz$ to truncate the UWB channels. Then zero-padding is used to make the subbands have the same bandwidth as the original channel.

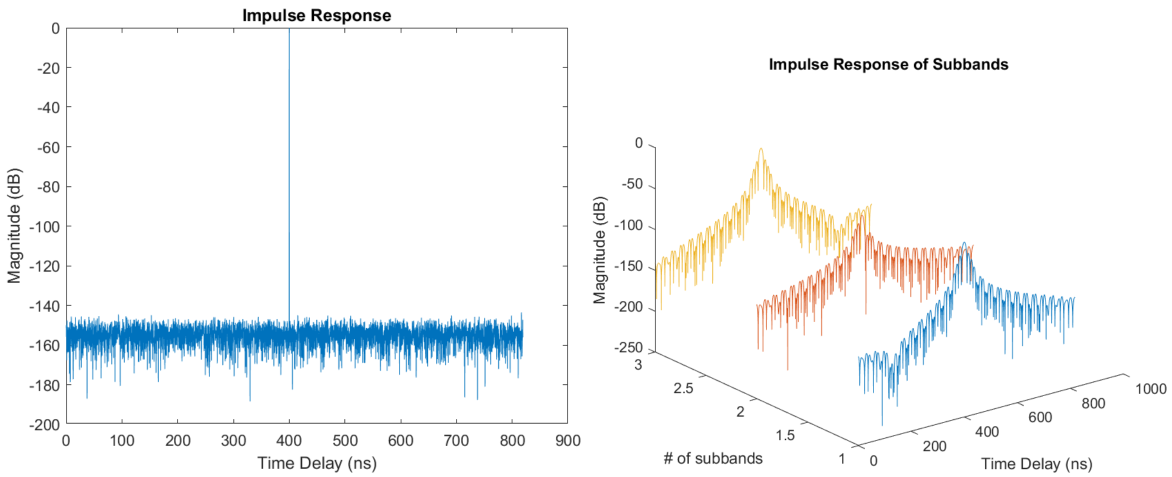

Figure 6.1: Impulse Responses of One Arrival Path Signal (Left) and Subbands (Right, one case when $\Delta f = BW_{sub} = 60MHz$)

According to equation (5.5), when there is only one arrival path in the CIR, no matter how we choose the different way to obtain the subbands, the subbands will also only have one arrival path, which means there is only one time point where the impulse response reaches the peak, same as the time delay of the direct path at original UWB CIR. In this case, when $\tau = 400ns$, the phase rotation can be fully compensated by $e^{j2\pi\Delta f\tau}$ and the covariance will be 1 whatever the Δf changes.

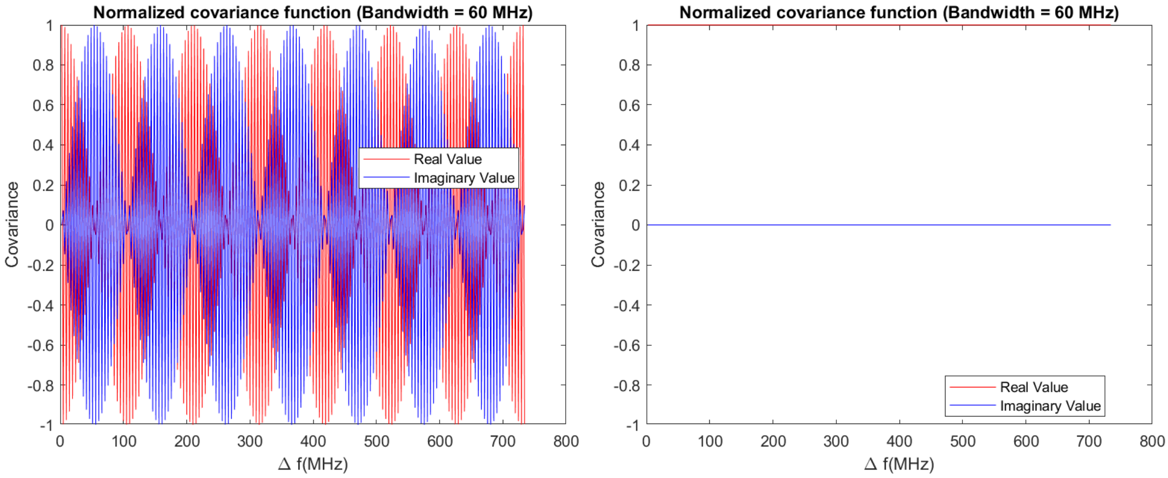

Figure 6.2: The covariance ρ_1 change versus Δf at 200ns (left) and 400ns (right)

From figures 6.2 and 6.3, we can find that at the arrival path delay, the covariance is always at 1 whatever Δf changes as expected. All the subbands are completely correlated at the time delay 400 ns. And also we notice that at 200 ns, the covariance changes rapidly when the Δf changes. Since the CIR only shows one path, the phase rotation between adjacent subbands CIRs will be the same, equals to $e^{j2\pi\Delta f\tau}$ where $\tau = 400ns$. But we actually use $\tau = 200ns$ to compensate the phase rotation based on equation (5.12) we proposed , resulting that we can not fully compensate the phase rotation and also introduce an inference which will change with Δf.

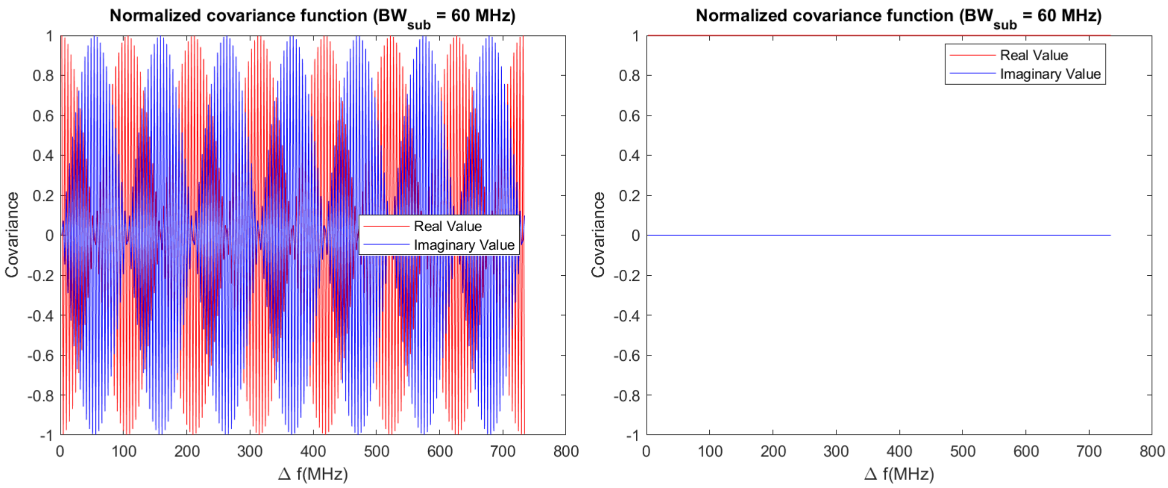

Figure 6.3: The covariance ρ_2 change versus Δf at 200ns (left) and 400ns (right)

Since we already know the phase rotation when the CIR only shows one path, a little change can be made on the covariance to validate our assumption that the phase rotation between adjacent subband CIRs will be the same when the CIR only shows one path inside the window-size time domain.

Then the key part of nominator of covariance becomes

$$
\begin{aligned}
&h_{bbk}(\tau)(h_{bb(k+1)}(\tau)e^{j2\pi\Delta f\tau_{l_2}})^* \\
&=\sum_{l_1=1}^{L} a_{l_1}e^{-j2\pi f_{c_k}\tau_{l_1}}w(\tau-\tau_{l_1})(\sum_{l_2=1}^{L} a_{l_2}e^{-j2\pi f_{c_k}\tau_{l_2}}w(\tau-\tau_{l_2})e^{-j2\pi\Delta f\tau_{l_2}}e^{j2\pi\Delta f\tau_{l_2}})^* \\
&=\sum_{l_1=1}^{L}\sum_{l_2=1}^{L} a_{l_1}a_{l_2}e^{-j2\pi f_{c_k}(\tau_{l_1}-\tau_{l_2})}w(\tau-\tau_{l_1})w(\tau-\tau_{l_2})
\end{aligned}
\tag{6.2}
$$

where τ_{l_2} is the time delay of the direct path, which in this example is 400 ns.

Rather than using measured time delay τ to compensate the subbands, here we directly use the $\tau_{l_2} = 400ns$ to compensate the phase rotation. It can be seen that the phase rotation is fully compensated, which means we get rid of interference item related to Δf. If our assumption is right, the covariance will be 1 inside the window-size time domain since two adjacent CIRs will be the same after compensation, here we take the covariance at $\tau = 401ns$, as shown in 6.4 and 6.5.

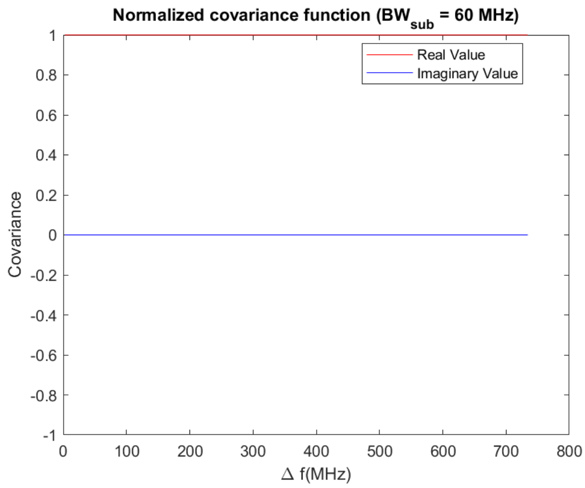

Figure 6.4: Covariance ρ_1 at 401ns

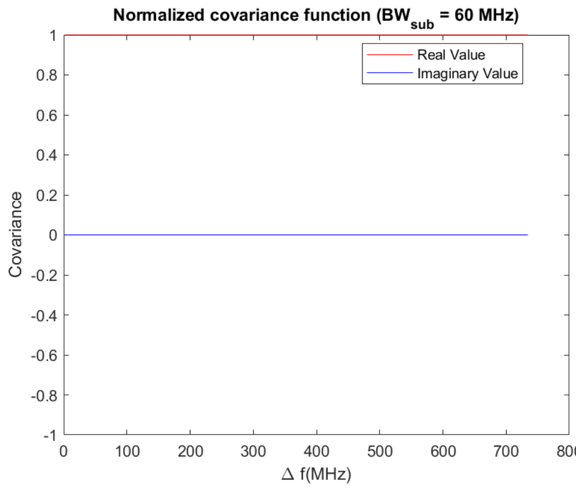

Figure 6.5: Covariance ρ_2 at 401ns

The results show that the time point around 400 ns also has the same phase rotation when the CIR of the UWB channel only shows the direct path. With no interference caused by other paths, the subbands will be fully correlated inside the window-size time domain.

In what follows, we will calculate the results when the CIR has more paths. Known that smaller bandwidth leads to a smaller time resolution, resulting in the loss of the ability to distinguish close-in paths, we would like to analyse the CIR with close-in paths and also paths that are far apart. Then given a CIR as shown in figure 6.6 with three paths at 12ns, 16ns, and 110ns separately.

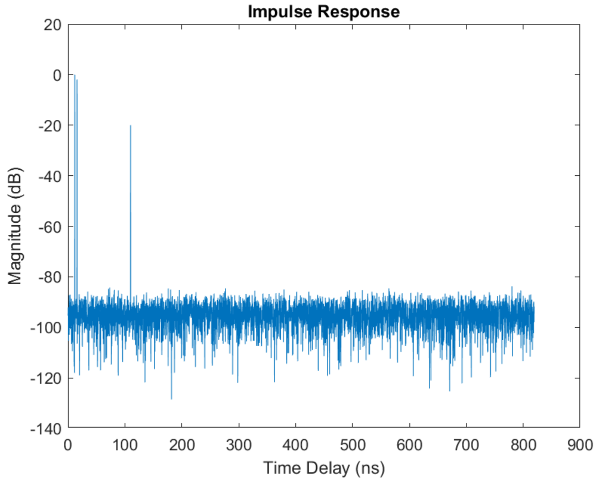

Figure 6.6: Impulse responses of three arrival path signal(arrive at 12ns, 16ns, 110ns)

Then we calculate the covariance at 12ns, 16ns, 110ns based on two methods separately, the results are shown in figure 6.7 and 6.8.

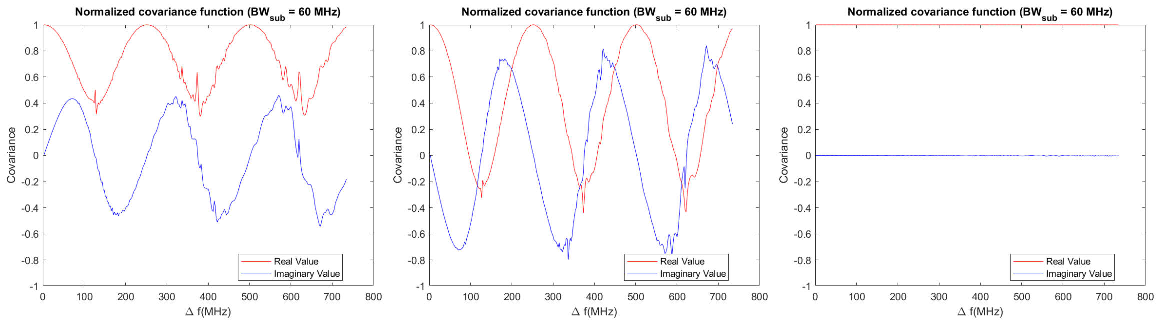

Figure 6.7: The covariance ρ_1 change versus Δf at 12ns (Left), 16ns (Middle) and 110ns(Right)

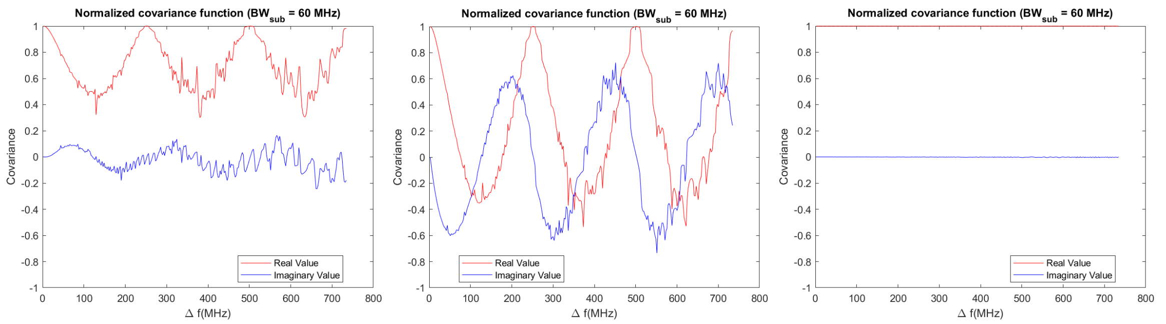

Figure 6.8: The covariance ρ_2 change versus Δf at 12ns (Left), 16ns (Middle) and 110ns (Right)

We notice that this two methods actually have similar results, the covariance ρ_2 is always slightly smaller than ρ_1, and the fluctuations of the curve are also similar.

Therefore, we will focus on the analysis of the covariance ρ_1 in the following simulations.

Here the the bandwidth of window function is 60 MHz, which means the time resolution is around 16.6 ns, resulting that subbands can not distinguish the paths where the time difference between them is smaller than 16.6 ns. The fluctuations of the curves in the first two figures are obviously due to the influence of the adjacent paths which only has a 4 ns difference. Conversely, the covariance of the third path stays at 1 since this path is far enough from the first two. Theoretically, there is 4ns difference between first two paths, if we want to get rid of the multipath interference, the bandwidth of the subbands should be larger than 250 MHz, then the fluctuations will disappear. To validate this, the results of the covariance change versus Δf at 12ns when the bandwidth of Window function is 120MHz, 240MHz and 300MHz is shown in figure 6.9.

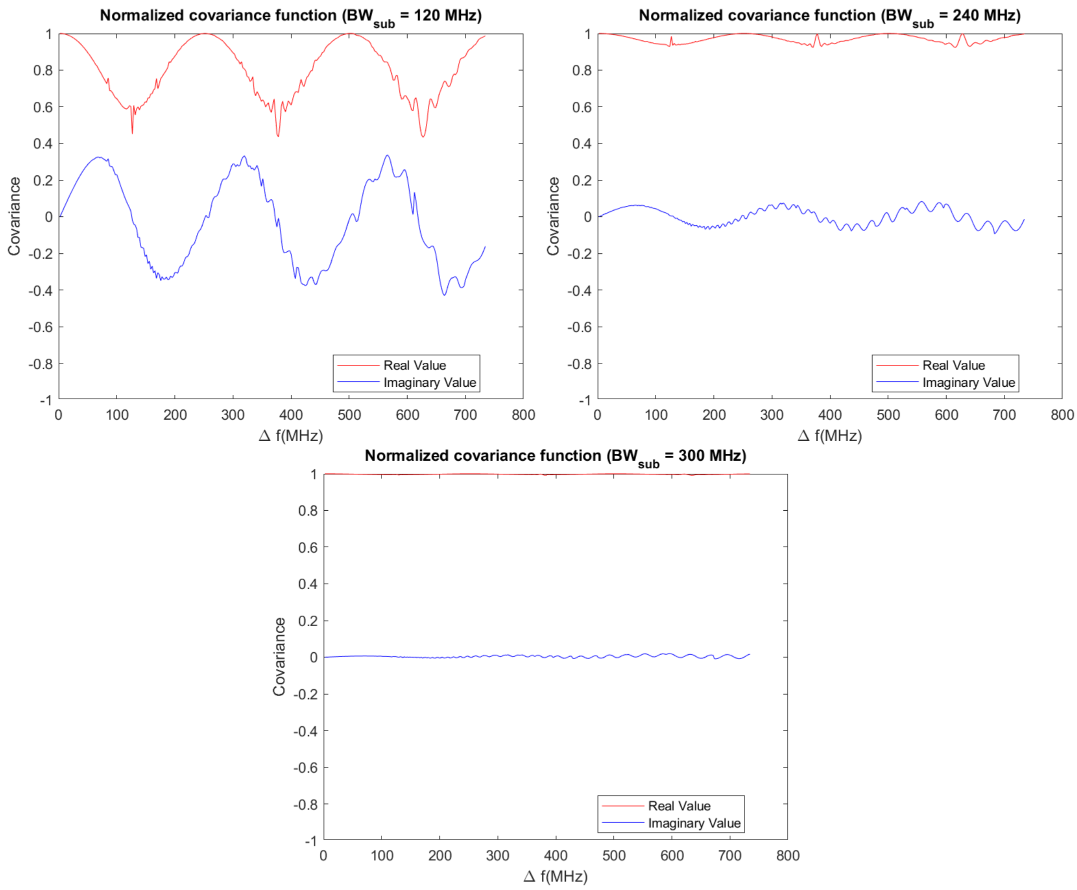

Figure 6.9: The Covariance ρ_1 change versus Δf at 12ns when the bandwidth of Window function is 120MHz, 240MHz and 300MHz

The results shown in figure 6.9 agrees with the analyse above. With the increase of the effective bandwidth, the covariance at the delay of arrival path becomes stable and stays at a high level close to 1. However, we should notice here in the given impulse response, the first two peaks have the same magnitude, which will bring a large interference to each other. In real life, the reflected paths will be lower than the direct path. Thus, the covariance of direct path will not be affected as much as this result shows.

Next, some measured CIRs will be given, the results based on (5.14) in practice will be discussed.

6.3 Measurements setup

The real UWB channels are measured over a frequency band of $BW = 5GHz$ with a center frequency 7.5 GHz at 4096 discrete frequency points collected from on the second floor of the B wing of the Kennedy campus of the AZG, Kortrijk Belgium [7].

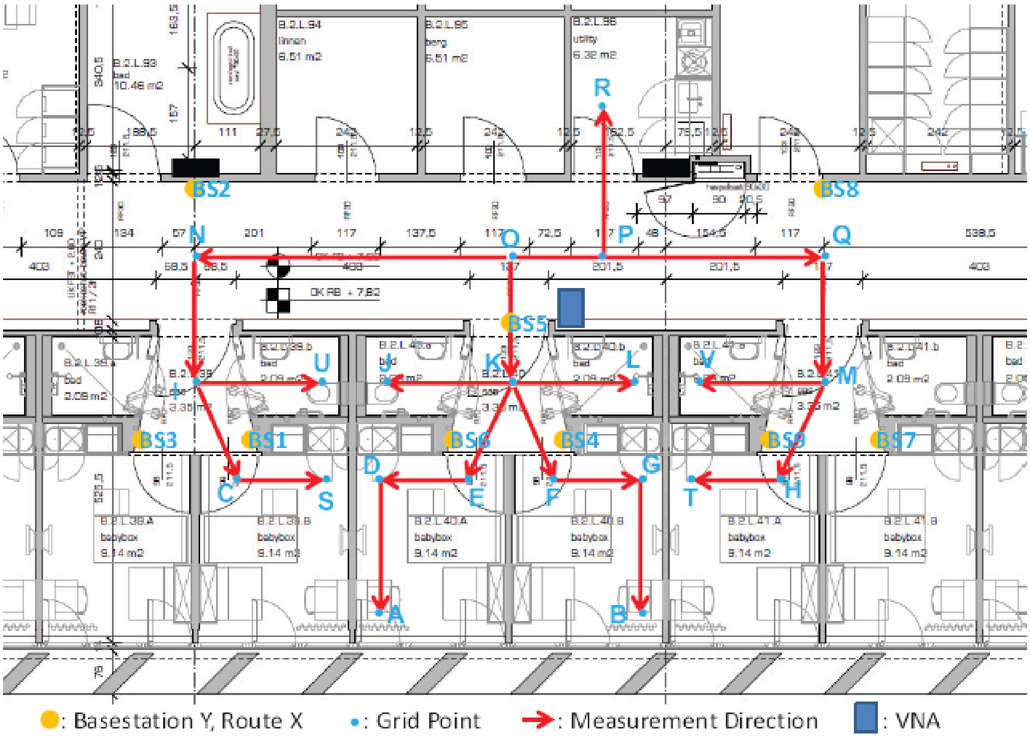

Figure 6.10: Environment floor plan, anchor positions and measurement segments [7]

The floor plan is shown in 6.10. For the measurements, with all doors open, no completely enclosed spaces in the entire measurement environment, 9 stationary antennas from BS1 to BS9 are placed in different places on the second floor and can be reached from anywhere on this floor without modifying the environment. An agent antenna will move on a fixed route during the measurement, and a 4-port vector network analyzer is used here, the channels between the agent and three stationary antennas are measured at once at each position. Therefore 9 anchor positions will be realized by repeating the same operation three times. Multiple measurements will be done to guarantee the stability of the whole data-collecting procedure. Based on collected data, the frequency domain transfer function of the channel from agent to each anchor will be deduced.

6.4 Measured channel impulse response

Since we already know that if two paths are close to each other, there will be interference, some measured channels where the direct path as well as some reflection paths are very obvious and not close to each other will be given. We will analyse the covariance and frequency dependence of these paths.

And from the equation (6.1), we already know that if CIRs show multiple paths, there will be an interference item related to Δf, and this interference can be reduced by the window function.

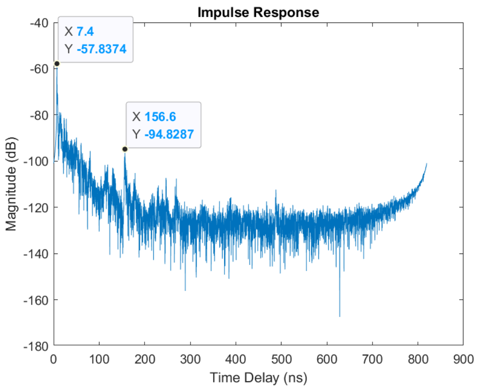

(a) CIR 1

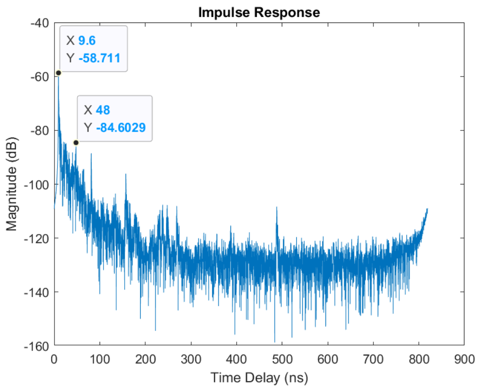

(b) CIR 2

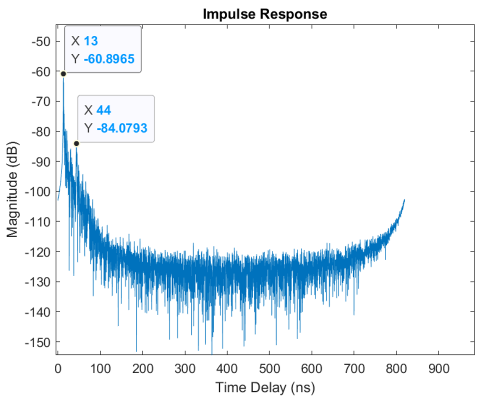

(c) CIR 3

Figure 6.11: Three Impulse Responses which shows distinct direct path and some reflections

From above three impulse responses, we can find that there are not too much reflections close to the direct path. In figure 6.11(a), the direct path arrives at 7.4 ns and there is a reflected path at 156.6 ns, the covariance at these two time points will be calculated with different bandwidths window functions. Likewise, in the figure 6.11(b) and 6.11(c), we can find the direct paths at 9.6 ns and 13 ns, reflected paths at 48 and 44ns, and the covariance will be calculated at these path delays.

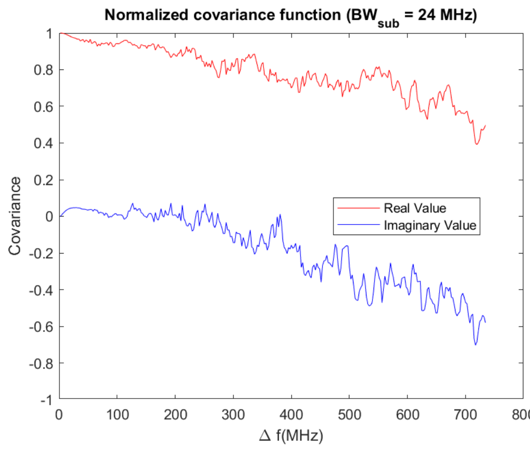

(a) When $BW_{sub} = 24MHz$ at 7.4 ns

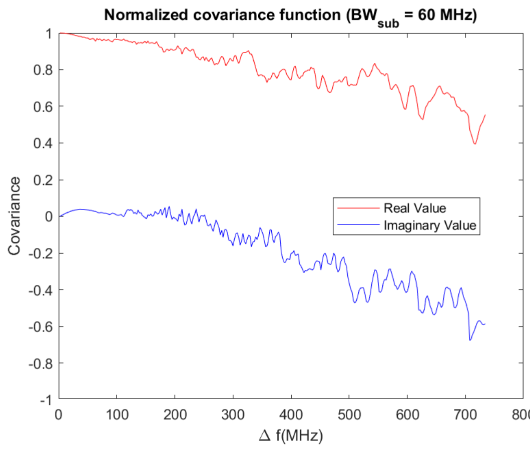

(b) When $BW_{sub} = 60MHz$ at 7.4 ns

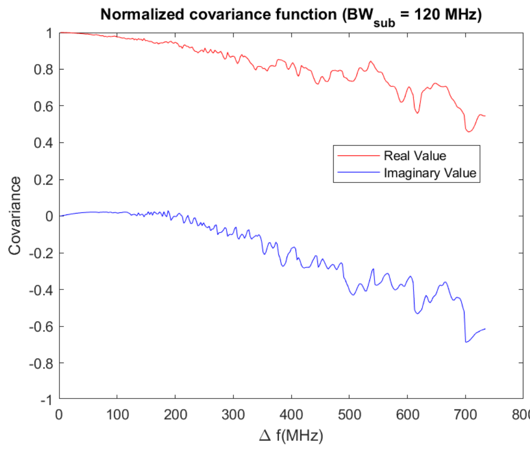

(c) When $BW_{sub} = 120MHz$ at 7.4 ns

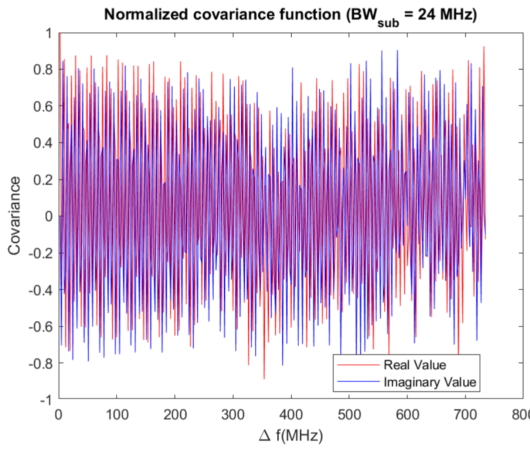

(d) When $BW_{sub} = 24MHz$ at 156.6 ns

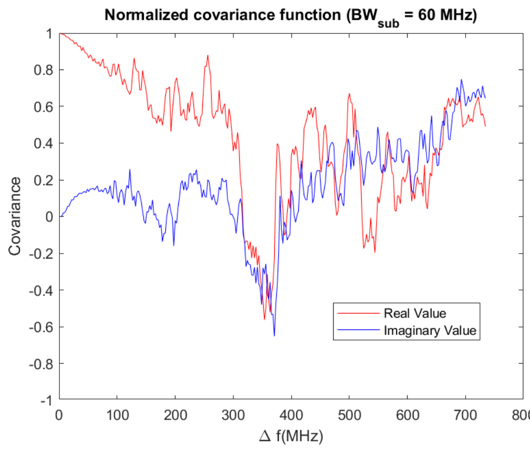

(e) When $BW_{sub} = 60MHz$ at 156.6 ns

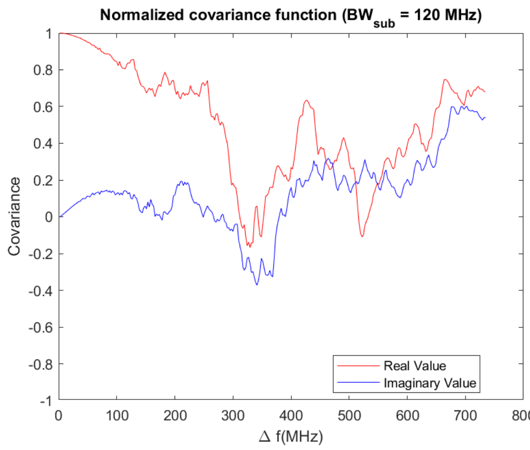

(f) When $BW_{sub} = 120MHz$ at 156.6 ns

Figure 6.12: Covariance change versus Δf of CIR 1

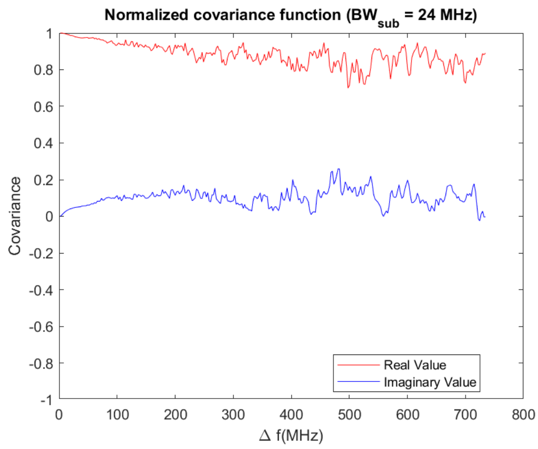

(a) When $BW_{sub} = 24MHz$ at 9.6 ns

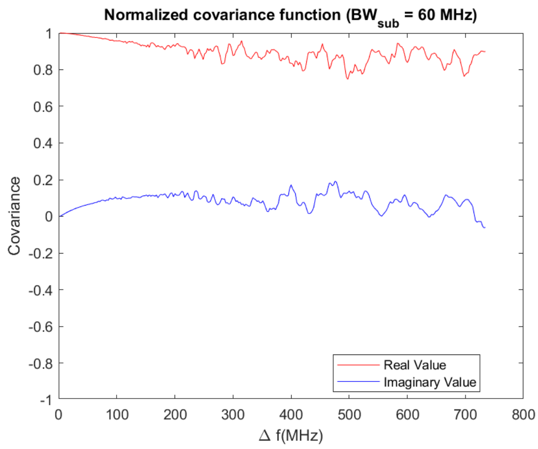

(b) When $BW_{sub} = 60MHz$ at 9.6 ns

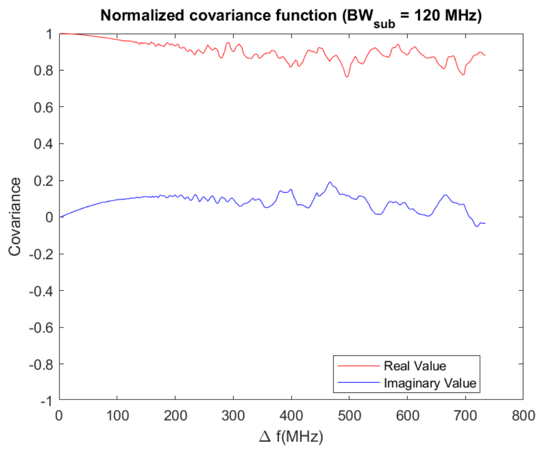

(c) When $BW_{sub} = 120MHz$ at 9.6 ns

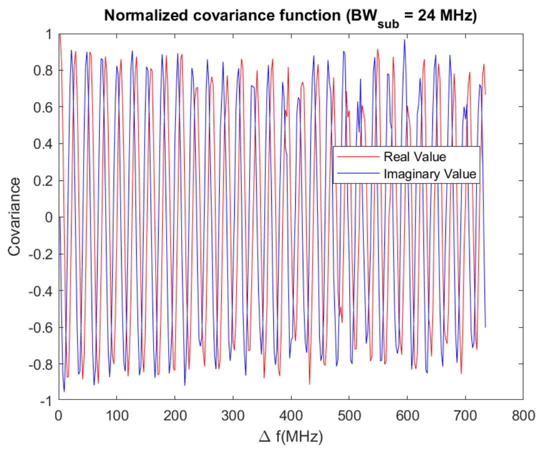

(d) When $BW_{sub} = 24MHz$ at 48 ns

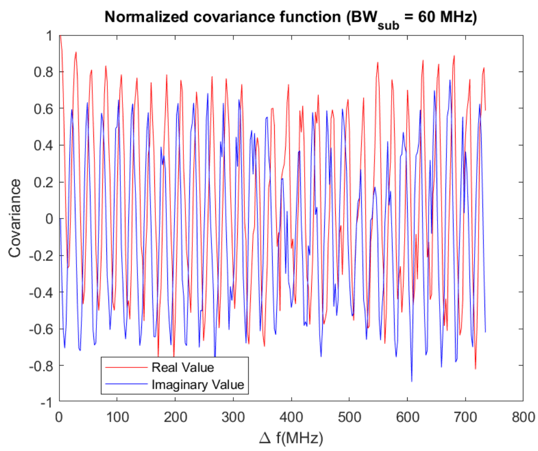

(e) When $BW_{sub} = 60MHz$ at 48 ns

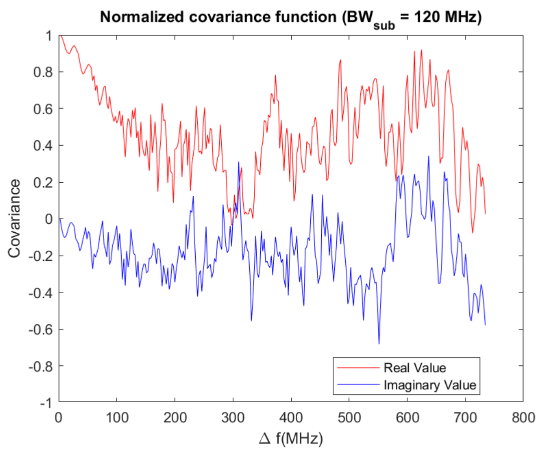

(f) When $BW_{sub} = 120MHz$ at 48 ns

Figure 6.13: Covariance change versus Δf of CIR 2

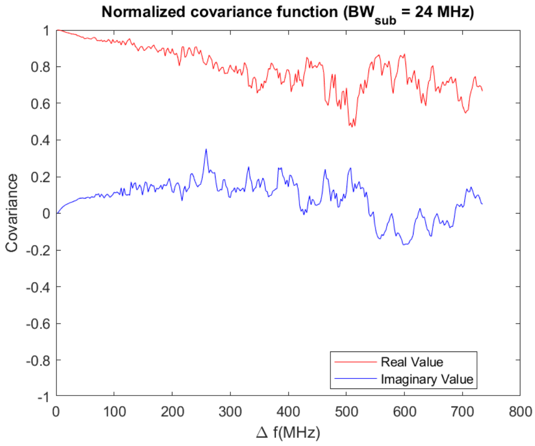

(a) When $BW_{sub} = 24MHz$ at 13 ns

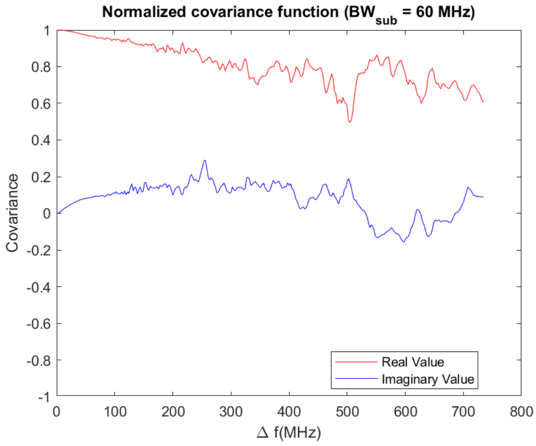

(b) When $BW_{sub} = 60MHz$ at 13 ns

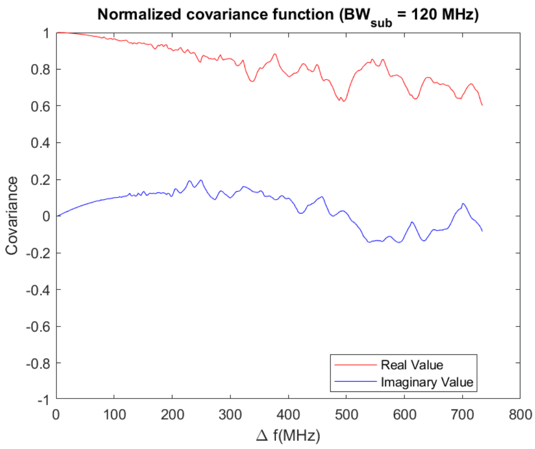

(c) When $BW_{sub} = 120MHz$ at 13 ns

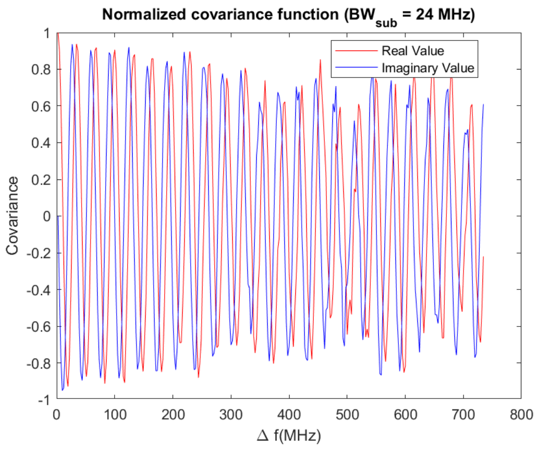

(d) When $BW_{sub} = 24MHz$ at 44 ns

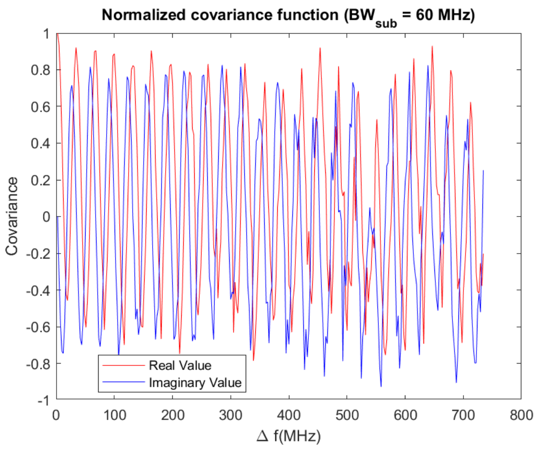

(e) When $BW_{sub} = 60MHz$ at 44 ns

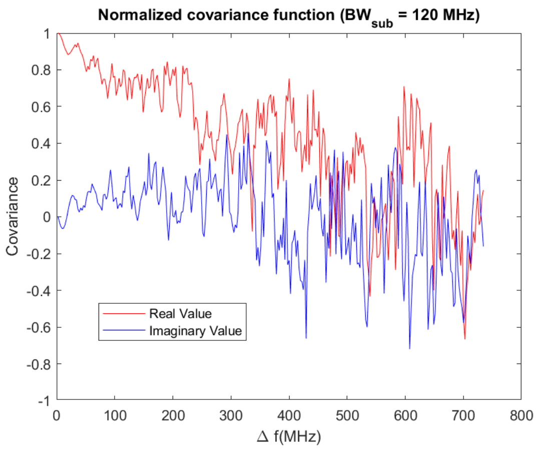

(f) When $BW_{sub} = 120MHz$ at 44 ns

Figure 6.14: Covariance change versus Δf of CIR 3

From the results of the three channels as shown in figures 6.12, 6.13 and 6.14, it is obvious that CIR will not be fully correlated when measured at different center frequencies since the covariance is not always 1, and we also can find that at the first arrival path, with the increase of Δf, the normalized covariance will decrease but stay at high level close to 1, which means the subbands are mostly correlated at direct path, but also we notice that when the Δf becomes large, the normalized covariance will change faster. In general, the covariances are larger than 0.5, so we can say that the direct paths of the subbands are correlated in time domain. As for the reflected path, the covariance drop to a low value which is smaller than 0.5 for smaller Δf. Therefore, these reflected paths of the subbands are uncorrelated. Consequently, the correlation of the direct path is maintained over larger frequency distances than that of reflected paths.

In addition, from the results, we can also find that in the direct path, when we increase the Δf, the trend of the curve will not change, but there will be a lot small jagged fluctuations on the curve, which will be smoother when the bandwidth of window function increase. As we analysed before, larger bandwidth of window function leads to higher time resolution, which can better filter out the interference caused by nearby paths caused by reflection or noise. And notice that there are reflected paths close to the direct path, the magnitudes of them are much lower than the direct path. After the filtration of the window function in time domain, their impacts on the direct path be further reduced.

Furthermore, we can find that the covariance at reflected path delays actually show a similar phenomenon to the direct path when the bandwidth of window function changes. The curves become smoother because of the higher time resolution. As shown in figure 6.11(a), 6.11(b) and 6.11(c), the reflected path is surrounded by many paths of similar strength caused by noise. The low time resolution makes it impossible to get rid of this influence. As we analyzed in the second artificial UWB channel example, such a similar strengths shows in close-in paths can bring a serious impact. As the bandwidth increases and the time resolution becomes higher, we can see that a large part of the interfering paths are eliminated, but there are still a few interfering paths that cause the subbands in the reflected path to be uncorrelated. Next, we will calculate the result

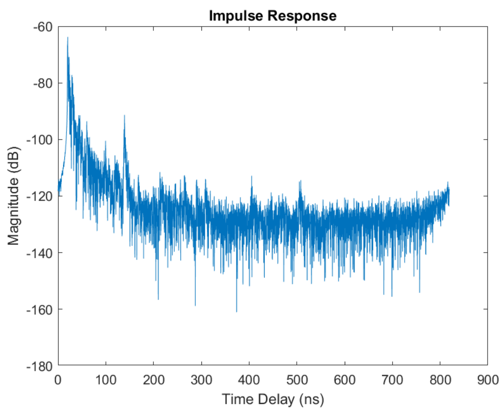

Figure 6.15: Channel impulse response with more reflected paths close to direct path

of the measured UWB channel where the CIR shows multiple paths, and there will be more paths close to the direct path. We will see how the covariance perform in this case. The CIR of the UWB channel is shown in figure 6.15.

The CIR shows that there are several reflected paths with high magnitudes close to the first arrival path, according to the analysis what we do, the direct path will be overwhelmed by the other paths. We calculated the covariance when $BW_{sub} = 120MHz, 240MHz, 480MHz$ at direct path (20.4ns) and reflected path (139.2ns).

It can be seen from the results shows in figure 6.16 that the covariance is lager than 0.5 in general when we change the bandwidth of the window function, thus the subbands are correlated for the direct path. And in reflected path, the subbands are correlated for small Δf and not correlated when Δf increase.

Compared to the results in figures 6.12, 6.13 and 6.14, we can find that in the direct path, the covarince shows larger change when Δf increases, which is because there are more paths close to the direct path. When the bandwidth of window function increases, more interference caused by these path is eliminated. For the reflected path, the covariance changes much faster, and subbands become uncorrelated at early stage.

6.5 Conclusion

To sum up, in this section, we validate the proposed covariance methods. And based on the results of the measured UWB channels subbands covariances, we analyse the frequency dependence of the CIR of subbands for different path delays. The two covariance methods both can have a good performance when there are multiple paths, even if the phase of subbands can not be fully compensated when there are multiple paths, most impact caused by reflected paths can be filtered out and reliable result can be found.

From the measured UWB channels, we can find that covariance for direct path is greater than 0.5, when indicates these subbands are correlated for direct path. For reflected paths, these subbands are correlated when Δf is small. In general, the correlation of the direct path is maintained over larger frequency distances than that of reflected paths. In addition, increase of the bandwidth of subbands can reduce more interference caused by other paths.

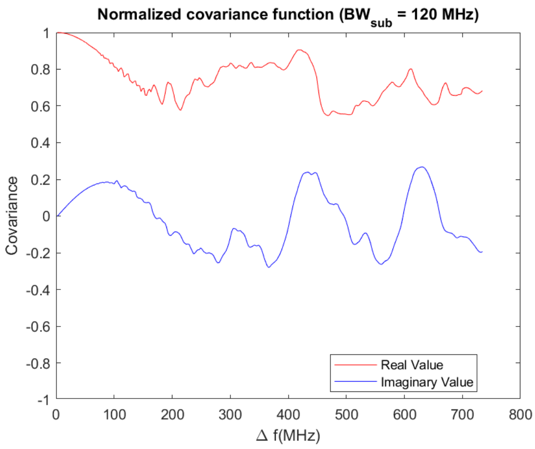

(a) When $BW_{sub} = 24MHz$ at 20.4 ns

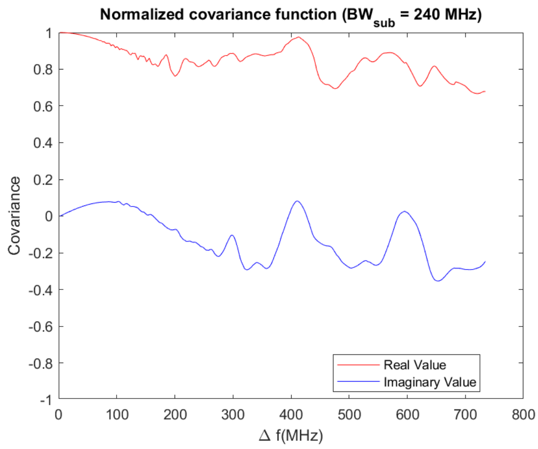

(b) When $BW_{sub} = 60MHz$ at 20.4 ns

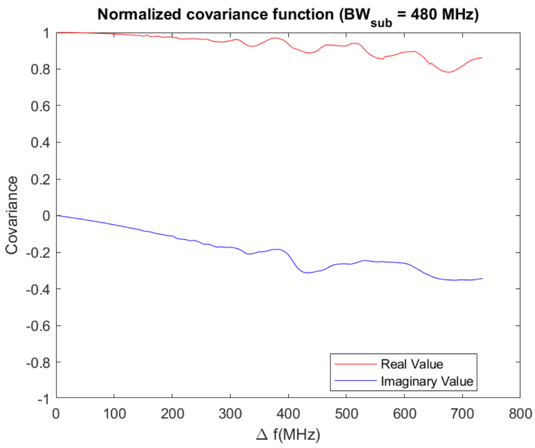

(c) When $BW_{sub} = 120MHz$ at 20.4 ns

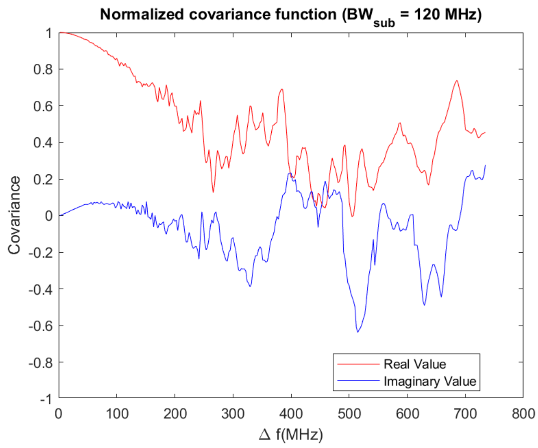

(d) When $BW_{sub} = 120MHz$ at 139.2 ns

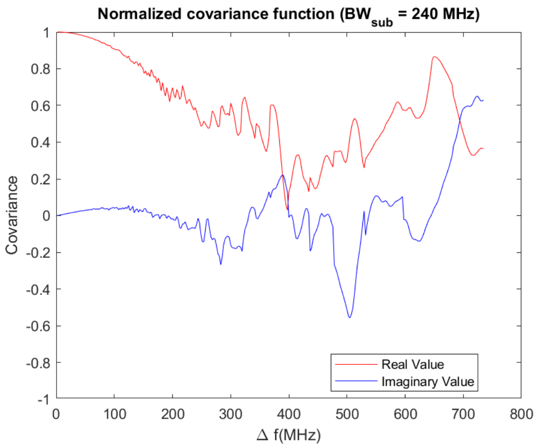

(e) When $BW_{sub} = 240MHz$ at 139.2 ns

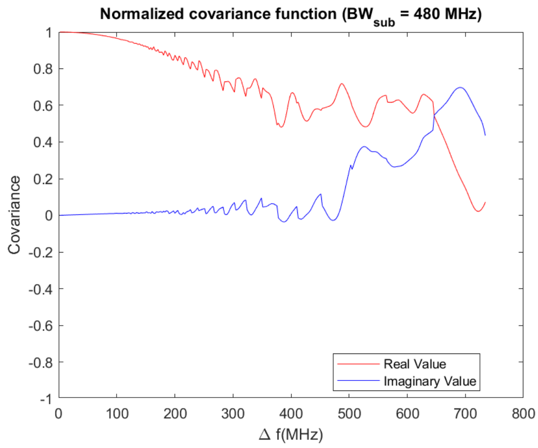

(f) When $BW_{sub} = 480MHz$ at 139.2 ns

Figure 6.16: Covariance change versus Δf

7 Conclusion & Future Work

7.1 Conclusion

In conclusion, this report can be divided into two topics. The first one is to find a optimal allocation of sparse subbands to constructed the UWB ranging signal with the same virtual bandwidth. And the second one is to figure out the frequency dependence of the subband channel impulse responses within a UWB channel.

For the first topic, two evaluation tools are proposed to assess the performance of virtual UWB signals. One is the Cramer-Rao Lower Bound and the other is the squared error of the auto-correlation function. Low CRLB and a small squared error should be obtained for a better performance. The sum of the sparse subbands is regarded as a virtual UWB signal, where two evaluation tools are applied to find a better a distribution of subbands over the virtual UWB bandwidth. The Newton's method is used to optimise the squared error function.

According to the simulation results, for a better performance of a signal consisting of sparse subbands in time delay estimation, the subbands should be close to the edges of the virtual bandwidth as much as possible. This results in a lower CRLB and a similar squared error of auto-correlation function to other allocation schemes.

For the second topic, a covariance model is proposed to measure the frequency dependence of the channel impulse response of subbands inside the UWB channel. To extract the subbands from the frequency domain measurements of an UWB channel, window functions with the same bandwidth which are centered at different frequencies are used to truncate the frequency domain measurements. Subband CIRs are obtained by using the inverse Fourier Transform on the frequency domain measurements of the subbands. The frequency difference between adjacent subbands is introduced as the independent variable. The covariance has been calculated by changing the frequency difference between subbands.

According to the results, it can be concluded that the channel impulse response will become different when measured at different center frequencies, where the difference increases with increasing the frequency separation of the subbands. The correlation of the direct path is maintained over larger frequency distances than that of reflected paths.

7.2 Future work

However, there is still a lot of work to do related to these two topics.

For the first topic.

- Find a more reasonable evaluation tool to measure the error of the auto-correlation caused by the constructed virtual signal. In our method, we focus on the general squared error which ignores how the error is generated, whether it is caused by side lobes or the main lobe of the auto-correlation. A more detailed method can be proposed, different weights can be assigned to different errors caused by ths side lobes and the main lobe.

- Not only focus on the the subband allocation, also find the trade-off between the TOA estimation accuracy of the virtual bandwidth, occupied bandwidth and more.

For the second topic,

- In the proposed covariance calculation method, the compensation of the phase rotation still can not perfectly avoid the interference under multiple paths situations, which is because of the reduced time resolution caused by narrow subband bandwidth. Therefore, some improvements can be made here to reduce the interference as much as possible, for example, we can use a sliding window to compensate the phase rotation around the direct path, or we can increase the bandwidths of several subbands to have a better time resolution.

- Try to find a model to compensate the frequency dependence within the UWB channel, which could also be used to improve the TOA estimation accuracy with an only partly known UWB channel.

Appendix A

Auto-correlation

For the correlation function, we can have

$$\begin{aligned} R_x(\tau) &= \mathcal{F}^{-1}\left\{\sum_{k=1}^{K} |X_k(f)|^2\right\} \\ &= \sum_{k=1}^{K} \mathcal{F}^{-1}\left\{P_{x_k}(f)\right\} = \sum_{k=1}^{K} R_{x_k}(\tau) \end{aligned} \tag{A.1}$$

Thus the auto-correlation function of the virtual signal consisting of a number of subbands can be written as the sum of the respective auto-correlation functions of the individual subband signals. For each subband, the auto-correlation function $R_{x_k}(\tau)$ could be written as

$$\begin{aligned} R_{x_k}(\tau) &=< x_k^*(t) x_k(t+\tau) > \\ &=< \left(x_k^{bb}\right)^* (t) e^{-j2\pi f_{a_k} t} x_k^{bb}(t+\tau) e^{j2\pi f_{a_k}(t+\tau)} \Big\rangle \\ &=< \left(x_k^{bb}\right)^* (t) x_k^{bb}(t+\tau) e^{j2\pi f_{a_k}\tau} > \\ &=< \left(x_k^{bb}\right)^* (t) x_k^{bb}(t+\tau) > e^{j2\pi f_{a_k}\tau} \\ &= R_{x_k^{bb}}(\tau) e^{j2\pi f_{a_k}\tau} \end{aligned} \tag{A.2}$$

From (A.1) and (A.2), we have

$$\begin{aligned} R_x(\tau) &= \sum_{k=1}^{K} R_{x_k}(\tau) \\ &= \sum_{k=1}^{K} R_{x_k^{bb}}(\tau) e^{j2\pi f_{a_k}\tau} \end{aligned} \tag{A.3}$$

Bibliography

[1] Luca Giugno and Marco Luise. Optimum pulse shaping for delay estimation in satellite positioning. In *2005 13th European Signal Processing Conference*, pages 1–6, 2005.

[2] Francesca Zanier, Giacomo Bacci, and Marco Luise. Criteria to improve time-delay estimation of spread spectrum signals in satellite positioning. *IEEE Journal of Selected Topics in Signal Processing*, 3(5):748–763, 2009.

[3] M Paonni, JT Curran, M Bavaro, and J Fortuny-Guasch. Gnss meta signals: Coherently composite processing of multiple gnss signals. In *Proceedings of the 27th International Technical Meeting of the Satellite Division of The Institute of Navigation (ION GNSS+ 2014)*, pages 2592–2601, 2014.

[4] Andreas F Molisch. Ultra-wide-band propagation channels. *Proceedings of the IEEE*, 97(2):353–371, 2009.

[5] Naveed Iqbal, Jian Luo, Christian Schneider, Diego Dupleich, Stephan Haefner, Robert Müller, and Reiner. S. Thoma. Frequency and bandwidth dependence of millimeter wave ultra-wide-band channels. In *2017 11th European Conference on Antennas and Propagation (EUCAP)*, pages 141–145, 2017.

[6] Wasim Q Malik, David J Edwards, and Christopher J Stevens. Frequency dependence of fading statistics for ultrawideband systems. *IEEE Transactions on Wireless Communications*, 6(3):800–804, 2007.

[7] J Romme, JHC van den Heuvel, G Dolmans, G Selimis, K Philips, and H De Groot. Measurement and analysis of uwb radio channel for indoor localization in a hospital environment. In *2014 IEEE International Conference on Ultra-WideBand (ICUWB)*, pages 274–279. IEEE, 2014.

[8] S. M. Kay. *Fundamentals of Statistical Signal Processing: Estimation Theory*. Prentice Hall, 1997.

[9] Jeroen C. J. Koelemeij Gerard J. M. Janssen, Christian C. J. M. Tiberius. Concept white paper on time-of-arrival estimation using coherent sparse subband signals. unpublished, 2020.

[10] F. Zanier and M. Luise. A new look into the issue of the cramér-rao bound for delay estimation of digitally modulated signals. In *2009 IEEE International Conference on Acoustics, Speech and Signal Processing*, pages 3313–3316, 2009.